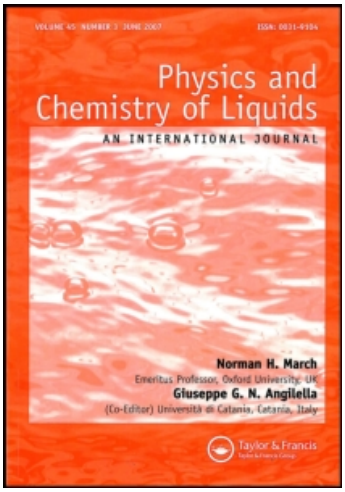


## Physics and Chemistry of Liquids

Publication details, including instructions for authors and subscription information:
http://www.informaworld.com/smpp/title~content=t713646857

# Atomic Transport in Liquids

T. Gaskell[a]; U. Balucani[b]; R. Vallauri[b]
[a] Department of Physics, The University, Sheffield, UK [b] Istituto di Elettronica Quantistica del Consiglio Nazionale delle Ricerche, Florence, Italy

**To cite this Article** Gaskell, T. , Balucani, U. and Vallauri, R.(1989) 'Atomic Transport in Liquids', Physics and Chemistry of Liquids, 19: 4, 193 — 239
**To link to this Article: DOI:** 10.1080/00319108908028445
**URL:** http://dx.doi.org/10.1080/00319108908028445

*Phys. Chem. Liq.*, 1989, Vol. 19, pp. 193–239
Reprints available directly from the publisher
Photocopying permitted by license only



# REVIEW ARTICLE
# Atomic Transport in Liquids

T. GASKELL

*Department of Physics, The University, Sheffield S3 7RH, UK.*

U. BALUCANI and R. VALLAURI

*Istituto di Elettronica Quantistica del Consiglio Nazionale delle Ricerche, 1-50127 Florence, Italy.*

*(Received 5 January, 1989)*



The topics discussed are:

i) The representation of experimental atomic transport coefficient data in simple liquids with respect to temperature and density, the emphasis being on self-diffusion and shear viscosity.

ii) The theoretical framework and the derivation of expressions for the coefficients in terms of Green Kubo integrands.

iii) Computer simulation data for the rigid sphere, Lennard-Jones and liquid metal-like systems.

iv) Rigid sphere dynamics and the rigid sphere fluid as a reference system for atomic transport in liquids.

v) Mode-coupling theory and interrelationships between coefficients.

We conclude that along the saturated vapour pressure curve the temperature dependence of the shear viscosity coefficient, $\eta$, for liquid metals is *not* the same as that of its counterpart in the inert gas liquids, according to the available experimental data. In addition, for the data examined a power law in $T$ is a more appropriate description than an Arrhenius expression. The situation is more confused for the self-diffusion coefficient, $D$. For the saturated liquid, a linear dependence can be claimed for Ar and some liquid metal data, but the evidence is not conclusive. To develop a coherent and comprehensive understanding of the transport mechanism more extensive diffusion data is essential.

We suggest, also, a more *systematic* approach to the determination of transport coefficients in computer simulation studies, particularly for liquid metal-like systems. On the theoretical front, in spite of an established framework, realistic calculations of atomic transport properties of liquids (on the scale required) are rare. Mode-coupling theory, we believe, offers the opportunity of progress here. We comment, finally, on interrelationships between coefficients and give a derivation of the Stokes-Einstein relation between $D$ and $\eta$ from a microscopic viewpoint.

KEY WORDS: Transport coefficients, Green-Kubo integrands, computer simulation, rigid sphere reference system, mode-coupling theory.

## 1 INTRODUCTION

We confine ourselves to a review of the atomic transport properties of classical monatomic liquids, and discuss the current experimental and theoretical situation in this 'simplest' area of liquid state physics.

There now exist systematic and reliable methods of calculating the structure and thermodynamic properties of simple liquids in terms of a given interatomic potential[1]. This is not the case for the transport properties. It is true that our understanding of the microdynamic behaviour of liquids has greatly increased over the last three decades, due to the development of (a) inelastic neutron scattering experiments, (b) computer simulation techniques for the study of models of liquids and (c) an appropriate theoretical framework. However, the translation of this understanding of the dynamics into confident predictions of, say, the temperature dependence of the shear viscosity, or diffusion, coefficient has still to be achieved. On the experimental side, a shortcoming is that data, in some important cases, tends to be available only for rather limited ranges of temperature. This is particularly so for the self-diffusion coefficient, due to the practical difficulties involved in the measurements. The result is that it is possible to obtain equally good descriptions of the temperature dependence of the data with (different) power laws, or, sometimes, an Arrhenius-type expression. The experimental situation for the shear viscosity is much better and we are able to reach more clear-cut conclusions.

We begin the review by summarizing the experimental methods which are used to measure self-diffusion, thermal conductivity and viscosity coefficients. The problems involved in the representation of the experimental data with respect to temperature and density are then discussed. Next, the theoretical framework is presented. The starting point is a generalized hydrodynamic point of view, involving the microscopic "conserved" variables and the derivation of a generalized Langevin equation. By this means, expressions for the transport coefficients are derived in terms of Green-Kubo integrands. In Section 4 we review computer simulation experiments, including the more recent non-equilibrium molecular dynamics techniques which has developed into a powerful means of studying transport properties. Applications of the theoretical framework to a rigid sphere fluid are then reported. The consequences of the instantaneous nature of the interaction, and the relevance of this model for our understanding of liquids is investigated. As with the thermodynamics, it is possible to make some progress by relating the transport properties of liquids to those of a rigid sphere reference system whose properties are assumed known. Despite their intrinsic importance we do not discuss kinetic theory developments nor their application to rigid sphere dynamics. Computer simulation data remains the basic reference system information for this type of approach, which can be useful in correlating experimental data, or predicting the values of transport coefficients.

Finally, mode-coupling methods, which attempt to describe microscopic dynamics in realistic model systems, are briefly considered. Simple applications are presented, leading to the derivation of expressions for the velocity and stress autocorrelation functions. Almost by definition, this approach describes the behaviour of a time-correlation function in terms of others, and can sometimes give insight into interrelationships between transport coefficients. By introducing the concept of a microscopic velocity field, an improvement in the mode-coupling result for the velocity autocorrelation function is first obtained. From this, we give a derivation of the Stokes-Einstein equation connecting the self-diffusion and the shear viscosity coefficients, and achieve some insight into the validity of this relationship at a microscopic level.

## 2 EXPERIMENTAL DETERMINATION OF ATOMIC TRANSPORT COEFFICIENTS

We consider, first, particle and heat diffusion processes. The diffusion of one fluid into another or the transfer of heat from one point in a fluid to another takes place as a result of concentration and temperature gradients respectively. The particle or heat flux, **J**, per unit area, per unit time, across a plane perpendicular to the flow is found empirically to have a linear dependence on the respective gradient. Hence we can write

$$\mathbf{J}_i = -D\nabla c_i \quad \text{(for particle diffusion, Fick's law)} \tag{2.1}$$

and

$$\mathbf{J}_q = -\lambda\nabla T \quad \text{(for heat transfer, Fourier's law)} \tag{2.2}$$

In the first equation $c_i$ is the concentration per unit volume of component $i$ and $D$ the inter-diffusion coefficient. In the second, $T$ refers to the temperature and $\lambda$ the thermal conductivity.

Continuity equations can be derived by considering the flux through an infinitesimal volume element of the fluid. These are readily obtained as

$$\frac{\partial c_i}{\partial t} + \nabla\cdot\mathbf{J}_i = 0 \tag{2.3}$$

and

$$nmCp\frac{\partial T}{\partial t} + \nabla\cdot\mathbf{J}_q = 0 \tag{2.4}$$

It is convenient to use the latter equations to eliminate the flux **J** from Eqs (2.1) and (2.2), giving

$$\frac{\partial c_i}{\partial t} = D\nabla^2 c_i \tag{2.5}$$

and

$$\frac{\partial T}{\partial t} = (\lambda/nmCp)\nabla^2 T \tag{2.6}$$

Equations (2.1), (2.2), (2.5) and (2.6) are of fundamental importance in the interpretation of experimental work on the atomic transport coefficients associated with diffusion and thermal conductivity.

### 2.1 *Self-Diffusion Coefficient*

We describe one practical application of Eq. (2.5) and mention others. To measure a self-diffusion coefficient, it is necessary to 'mark' or 'label' some of the particles, without changing their diffusive properties, and to identify the 'inter-diffusion' coefficient in (2.5) with the 'self-diffusion' coefficient. This labelling can be achieved, for example, by radioactive isotopic substitution. [The introduction of isotopes of a different mass means that the self-diffusion coefficient of the 'normal' liquid is not

strictly being measured. However, measurement errors are expected to exceed effects associated with isotopic mass differences—with the notable exception of liquid lithium[2].] Such a technique is used in the capillary-reservoir experiment[3], which has been responsible for a great deal of diffusion data on liquid metals. In this method, a narrow capillary, one end closed, is filled with the labelled species and lowered into a reservoir of inactive liquid. Diffusion of the labelled atoms takes place and after an appropriate time their concentration in the capillary is measured. If $c_0$ is the initial concentration of the marked atoms in the capillary and that in the reservoir zero, the solution of Eq. (2.5) for this essentially one dimensional case is[4]

$$c(z, t)/c_0 = (4/\pi) \sum_{n=0}^{\infty} (-1)^n/(2n + 1) \exp[-(2n + 1)^2\pi^2 Dt/4l^2] \cos[(2n + 1)\pi z/2l] \tag{2.7}$$

where $c(z, t)$ is the concentration at height $z$ above the bottom of the capillary, length $l$, after time $t$. The average concentration along the capillary is measured in practice, which, from Eq. (2.7) is given by

$$\bar{c}/c_0 = (8/\pi^2) \sum_{n=0}^{\infty} (-1)^n/(2n + 1)^2 \exp[-(2n + 1)^2\pi^2 Dt/4l^2] \tag{2.8}$$

When $Dt/4l^2$ is large enough, convergence of the series is rapid, and only the first term need be considered, so that

$$\bar{c}/c_0 = (8/\pi^2) \exp[-\pi^2 Dt/4l^2]$$

or

$$\ln(\bar{c}/c_0) = (-\pi^2 Dt/4l^2) + \ln(8/\pi^2) \tag{2.9}$$

Plotting $\ln(\bar{c}/c_0)$ versus time, $t$, at which the capillary is examined should produce a linear graph from which $D$ is determined from the slope. If convergence is not rapid enough, numerical fitting techniques may be used instead to obtain a value for $D$[5].

There are a number of potential sources of error in this method the most serious of which arises from the accumulation of solute atoms in the neighbourhood of the capillary exit. This would invalidate the boundary condition on which Eq. (2.7) is based, namely, that the concentration of labelled atoms at this point is zero. A correction for this effect can be attempted by using an increased effective capillary length $l + \Delta l$. Alternatively, the solution can be stirred to sweep away the diffusing tracer atoms as they emerge from the capillary. However, the choice of stirring speed is very important. It must be slow enough to prevent the development of turbulence which drags the fluid from the capillary[6]. Other, similar techniques are:

i) The long capillary method, in which half of the capillary is filled with isotopically enriched liquid and the other half with ordinary liquid. This technique has proved useful in high pressure studies of diffusion[7]. It has also been developed to allow continuous monitoring of the tracer atoms and applied to a range of liquid metals[8].

ii) The shear cell method, where the cell consists of several discs, which have a common axis of rotation, and which contain holes. These may be aligned to form a

capillary, or mis-aligned to break it into segments after a diffusion experiment. This would start with a thin layer of solute in the middle of the capillary. If $A$ is the initial concentration of solute per unit area, the appropriate solution of Eq. (2.5) is

$$c(z, t) = A(4\pi Dt)^{-1/2} \exp(-z^2/4Dt) \tag{2.10}$$

which gives the concentration of the solute as it diffuses in both directions. Any dissymmetry in the two profiles, due to convection, is easily detectable. The concentration profiles of the solidified segments are measured, as in other experiments, by chemical or radioactive analysis and $D$ determined by application of Eq. (2.10).

It should be stressed that the capillary technique is subject to the troublesome difficulties associated with convection effects. Rigney[9] has given a critical discussion of these for experimental work on atomic transport properties of liquid metals. More recently, Persson *et al.*[10] have reviewed this important topic and considered the development of new techniques to minimise the problems.

Nuclear magnetic resonance methods provide another source of information about diffusion in liquids. They involve either measurements of the spin lattice relaxation time or use of a spin-echo technique[6]. The former gives only relative values of the self-diffusion coefficient and requires a theory of the relaxation process. The latter, however, provides absolute values for $D$ and has the advantage that no assumptions concerning the mechanism of the diffusion process are needed. It involves measuring that part of the spin relaxation process due to the diffusion of spin orientated nuclei in a magnetic field gradient, after perturbation of the equilibrium distribution of nuclear magnetic moments by radio frequency energy pulses. For the simple liquids of interest here the accuracy is generally poorer than for the tracer methods, and liquid metals present special difficulties[9]. However, some elements have no convenient radioactive tracer. These include lithium, and the value for $D$ quoted in Table 5.2 was determined by NMR[11]. It refers to the diffusion of $^7$Li in natural Li which contains 92.57% $^7$Li.

In principle, $D$ can also be determined from experimental data of the incoherent component of the inelastic neutron scattering cross section. Larsson[12] has quite recently reviewed the possibilities and limitations of this type of approach.

### 2.2 *Thermal Conductivity*

In contrast to the concentration measurements of diffusion coefficients discussed above, a steady state technique using Eq. (2.2) is considered preferable for the determination of the thermal conductivity of a liquid. Amongst other reasons, the calculations required in nonsteady state methods are either very tedious or inaccurate, although this type of approach has been used[13].

The essentials of the method involve placing a layer of the liquid under investigation in a gap between either parallel plates or the annular gap between vertical concentric cylinders. Both types of geometry have been used[14,15], although the latter has certain practical advantages in the reduction of heat losses. It has been claimed, also, that for high pressure work particularly the restrictions on the geometry, imposed by the necessity to fit the cell into a high pressure vessel, make the cylinder method preferable[16]. A heater coil runs along the central axis of the inner cylinder, with a resistance calibrated as a function of temperature, and a temperature gradient,

$\nabla T$, maintained across the inner and outer cylinders. The heat energy, generated at the known rate, $Q$, is conducted radially outwards through the liquid layer. The application of Eq. (2.2) leads to the result that

$$\lambda = Q \ln(r_2/r_1)/(2\pi L \nabla T) \tag{2.11}$$

In this equation $L$ is the length of each cylinder and $r_1$ and $r_2$ ($r_2 > r_1$) the radii. Corrections to this simple expression are required in practice[16].

### 2.3 *Viscosity*

*a) Shear viscosity* Once again, there is choice between a steady and a non-steady state method. The first category includes capillary flow, falling ball or cylinder, and rotating cylinder techniques. The capillary flow method is very well known and conveniently used at room temperature and atmospheric pressure. At high pressures there are technical problems where visual observation is required. At low temperatures the necessity of pumping the liquid back to the viscometer head creates difficulties, although these have been overcome in different ways[17,18]. The pressure dependence of the shear viscosity coefficient is probably most easily determined by a damped oscillator technique, which falls into the second category. A form of oscillating disc viscometer[19], vibrating wire viscometer[20] or torsionally oscillating crystal viscometer[21] have been applied. A great deal of data on the inert gas liquids have been obtained in this way[21], although it has been pointed out that the results from the different sources do not always agree[19,21].

For liquid metals and their alloys, where thermodynamic conditions are generally more extreme and the liquids more reactive, a form of oscillating cup viscometer has had wide application. A right-circular cylindrical cup containing the liquid is suspended by a torsion fibre so that an oscillating pendulum is formed. A sealed cup prevents vapourization and reactions of the liquid metals with atmospheric gases. As with the other non-steady state methods, the theory of the cup viscometer involves both the equation of motion of a Newtonian fluid and that of the cup. These are respectively

$$nm\left\{\frac{\partial}{\partial t} + \mathbf{v}\cdot\nabla\right\}\mathbf{v} = -\nabla p - \nabla\cdot\boldsymbol{\sigma} + nmg \tag{2.12}$$

and

$$I\frac{d^2\theta}{dt^2} = L \tag{2.13}$$

In Eq. (2.12), $\mathbf{v}$ is the velocity of the fluid, $p$ the pressure, $\boldsymbol{\sigma}$ the stress tensor, and $g$ the gravitational acceleration; in (2.13) $I$ is the moment of inertia of the cup and $L$ the *total* torque on it. The drag of the liquid within the cup produces a contribution to the torque. This is expressed in terms of a component of the stress tensor and hence is proportional to the shear viscosity coefficient, $\eta$, and the velocity gradient of the fluid. Details of a treatment of these equations and their application to the experimental determination of viscosity are given, for example, by Wittenberg *et al*[22].

A comprehensive review of this method, along with alternative experimental techniques which have been used for liquid metals, has recently been published by Shpil'rain *et al.*[23]. The reader is referred to this reference for a critical discussion, and for the tabulation of recommended values of the shear viscosity of the liquid alkali metals over an extensive range of temperature.

*b) Bulk viscosity* Direct, independent, measurement of the bulk viscosity coefficient, $\eta_B$, appears not to be possible. However, the bulk viscosity, in combination with the shear viscosity and thermal conductivity, contributes to the attenuation of sound wave energy in a liquid. Experimental investigation of sound attenuation therefore allows an estimate of $\eta_B$ to be made, provided that $\eta$, $\lambda$ and the specific heats $C_P$ and $C_V$ for the liquid are already known.

The relevant theoretical results can be obtained from the theory of the density fluctuation spectrum outlined in Section 3. The half-width, $\Delta\omega$, of the Brillouin peaks (which represent propagating sound waves) is given by Eqs (3.32) and (3.37) which are consistent with a hydrodynamic treatment of the liquid. For a given wavevector the result is

$$\Delta\omega = \tfrac{1}{2}[(4\eta/3 + \eta_b)/nm + (\lambda/nmC_P)(\gamma - 1)]q^2 \tag{2.14}$$

with $\omega = c_s q$.

In these equations $c_s$ is the sound velocity, $C_P$ the specific heat per unit mass and $\gamma$ the specific heat ratio. In the hydrodynamic regime, where the wavelength of the propagating modes $\gg$ the interparticle separation, light scattering experiments (where possible) are an appropriate technique to investigate the dynamical behaviour of the density fluctuations. In principle, this type of investigation is one means of obtaining a value for $\eta_B$.

Fleury and Boon[24] have investigated the Brillouin spectrum for 5145 Å laser light scattered from liquid Ar at $T = 85$ K. The observed sound speed, $c_s = 850 \pm 4$ ms$^{-1}$ is close to the low-frequency value measured acoustically, $c_s = 853$ ms$^{-1}$. Unfortunately, numerical analysis of the line shapes, and an estimate of the bulk viscosity coefficient, was not carried out. Fluctuations in the instrumental width caused by the wandering of the single mode laser frequency, made such a process unreliable.

The alternative approach is to measure the sound attenuation coefficient, $\alpha$, when ultrasonic waves are transmitted through the liquid. Using the two expressions in Eq. (2.14), it is readily seen that this is given by

$$\alpha = (\omega^2/2c_s^3)[(4\eta/3 + \eta_B)/nm + (\lambda/nmC_P)(\gamma - 1)] \tag{2.15}$$

The extra factor of $c_s$ arises from conversion to attenuation per unit length. It follows that

$$\eta_B = (2\alpha nmc_s^3/\omega^2) - [4\eta/3 + (\lambda/C_P)(\gamma - 1)] \tag{2.16}$$

and the accuracy of the result depends on firm knowledge of thermodynamic and transport properties of the liquid under investigation. Naugle *et al.*[25] have measured the attenuation coefficient in liquid Ar at frequencies from 30 to 70 Mc s$^{-1}$ using a pulse-echo technique. They reported quite extensive results for $\eta_B$ with an estimated

error of $\pm 25\%$. Calculations of the required specific heat ratio from equation of state data was considered to be a significant source of error. Ultrasonic attenuation in liquid metals has also been measured[26], and the experimental techniques recently reviewed by Beyer[27]. There is an additional problem in metals, following from the fact that in Eq. (2.15) the conductivity component dominates the viscosity contribution to $\alpha$. Typically, it represents about 70–80% of the total. Because of this, there are obvious difficulties in an accurate determination of $\eta_B$ by means of Eq. (2.16). However, data for a number of metals are listed by Sharma[28].

### *2.4 Representation of Experimental Data*

Self-diffusion coefficients are difficult to measure accurately and the most extensive and reliable atomic transport data available in simple liquids is of the shear viscosity. It is appropriate, therefore to consider these data first.

One of the most widely used concepts in the representation of experimental transport coefficient data for viscosity (and diffusion) is that of an "activation energy". This followed from the observation that the temperature dependence of the viscosity of liquids could be fitted by the formula, $\eta = \eta_0 e^{E_v/kT}$, over the (rather limited) range of thermodynamic conditions usually investigated[29]. The parameters $\eta_0$ and $E_v$ are temperature independent, and by analogy with the Arrhenius equation for the chemical rate constants, $E_v$ is referred to as an activation energy (for viscous flow). There is now some extensive shear viscosity data available for the liquid alkali metals[23] to examine the concept further. Although Arrhenius plots can still be a useful practical way to represent the temperature dependence of $\eta$ over a restricted range of temperatures (in liquid metals, from the melting point to about twice the melting temperature), as Figure 2.1 shows the assumption of an Arrhenius law is not confirmed over a wider temperature range. However, if this type of expression is made more flexible by using a temperature-dependent prefactor, it can be used to fit the experimental data, and *extrapolate* the results to higher temperatures. This has been done for all the alkali data reported in Ref. 23. The equation takes the form

$$\eta = T^{-B} \exp[-A + C/T]$$

or

$$\ln(\eta) = -A - B\ln(T) + C/T \tag{2.17}$$

The parameters $A$, $B$ and $C$ are chosen by means of a least squares fitting procedure. For temperatures up to $\approx 1500$ K an accuracy of better than 5% is claimed. Up to 2000 K it is of the order of 10%.

Using the data, we have observed that for the alkali metals the fluidity, $\eta^{-1}$, has a simpler representation, namely an approximate (and so far unexplained) linear dependence on $\sqrt{T}$, as demonstrated in Figure 2.2. The temperature range extends from near the melting point to temperatures close to 2000 K, and we assume that the experimental data is for thermodynamic states along the saturated vapour-pressure curve. It is interesting to compare this with the viscous behaviour of saturated liquid argon. Haynes[21] has determined the viscosity from 85 K to 150 K, and over this range $\eta$ changes by an order of magnitude. In contrast to the alkali metals, the fluidity does

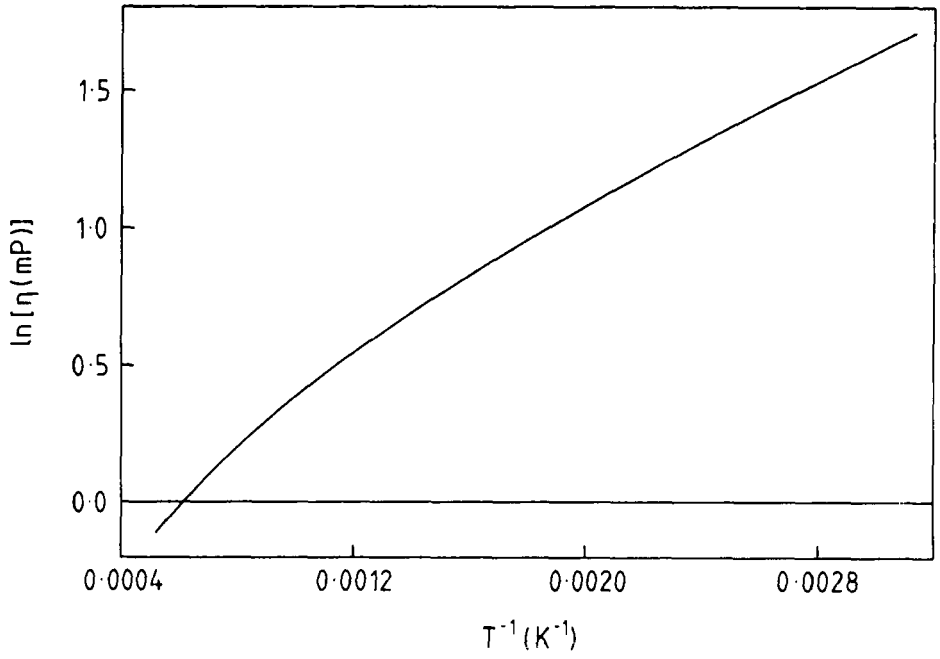


**Figure 2.1** Plot of $\ln[\eta(\text{mP})]$ against $1/T$ for liquid rubidium at saturated vapour pressure. Data from Shpil'rain *et al.*[23].



not vary linearly with $\sqrt{T}$. Over a temperature range from 85 K–120 K $\log(\eta)$ is approximately linearly-dependent on $T^{-1}$. Taborek *et al.*[30] have investigated the temperature dependence of the viscosity of a number of liquids in terms of a power-law behaviour, although their primary interest was in the supercooled region of the phase diagram. They suggest that $\eta^{-1/2}$ versus $T$ shows approximately linear behaviour for some simple liquids, including argon. We demonstrate the range of applicability in Figure 2.3, using Haynes' data. For the limited temperature range just referred to, the linearity is more striking than for the Arrhenius plot. When argon data is examined more carefully they find that the form

$$\eta = A(T/T_0 - 1)^{\mu} \tag{2.18}$$

describes the behaviour more precisely (if $\mu = -2$ this equation is consistent with our previous statement). In practice the value for $\mu$ depends on the liquid, but fluctuates about $-2$. The result for argon is shown in Figure 2.3 when we use the parameter values $A = 8.31$ mP, $\mu = -1.82$ and $T_0 = 30$ K. Unfortunately, the temperature range is too small in this case to appreciate properly the quality of the fit. This type of analysis is *not* appropriate for the liquid alkalis with a power law exponent $\approx -2$, a conclusion which is consistent with the investigations of Taborek *et al.* on the other liquid metals.

The transport coefficients of a rigid sphere fluid are determined entirely by the packing fraction. For liquids, one expects the transport properties to depend primarily

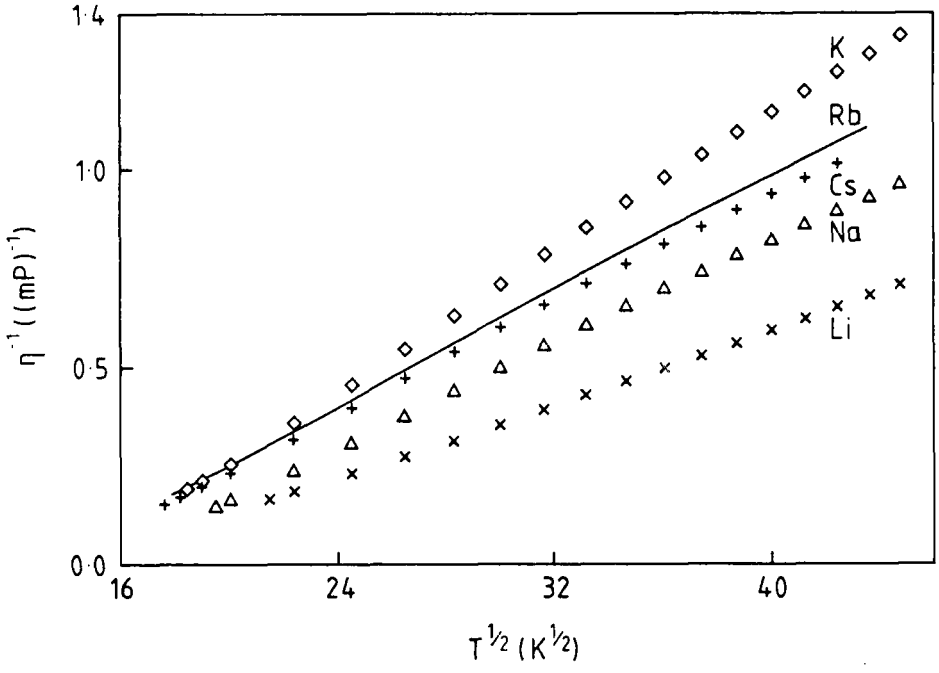


**Figure 2.2** Variation of fluidity with $T^{1/2}$ for five liquid alkali metals at saturated vapour pressure. Data from Shpil'rain *et al.*[23]



on the density. The density dependence too provides evidence against the idea of introducing an activation energy into the interpretation of viscosity data—by the observation that the fluidity of some simple liquids is a linear function of molar volume. Using this free volume concept, due to Batschinskii[31], enables one to write

$$\eta^{-1} = B(V - V_0)/V_0 \tag{2.18}$$

where $V_0$, the volume at which the fluidity becomes zero, may be regarded as the volume of the solid at the melting point. If true, this implies that there is no energy barrier to the movement of molecules but that the latter is determined by the available free volume only. Hildebrand[32] discusses this equation at some length, and gives examples of its applicability. Van Loef[33] has reported an investigation of the inert gas liquids (with the exception of $^4$He). He finds an approximate linear relationship between $\eta^{-1}$ and $V$ over a wide density range and for temperatures from the triple point to the critical temperature. However, the spread of data points at the higher end of the density range indicates that, along an isochore, the shear viscosity decreases with increasing temperature although the dependence is substantially less than $\sqrt{T}$. The data is presented in reduced form, the scales of length and temperature being those associated with a 6-12 Lennard-Jones potential, namely $\sigma$ and $\varepsilon/k_B$ respectively. From the results van Loef concludes that a corresponding states principle is obeyed for this linear relationship. Further study of Eq. (2.18), along isotherms, has been

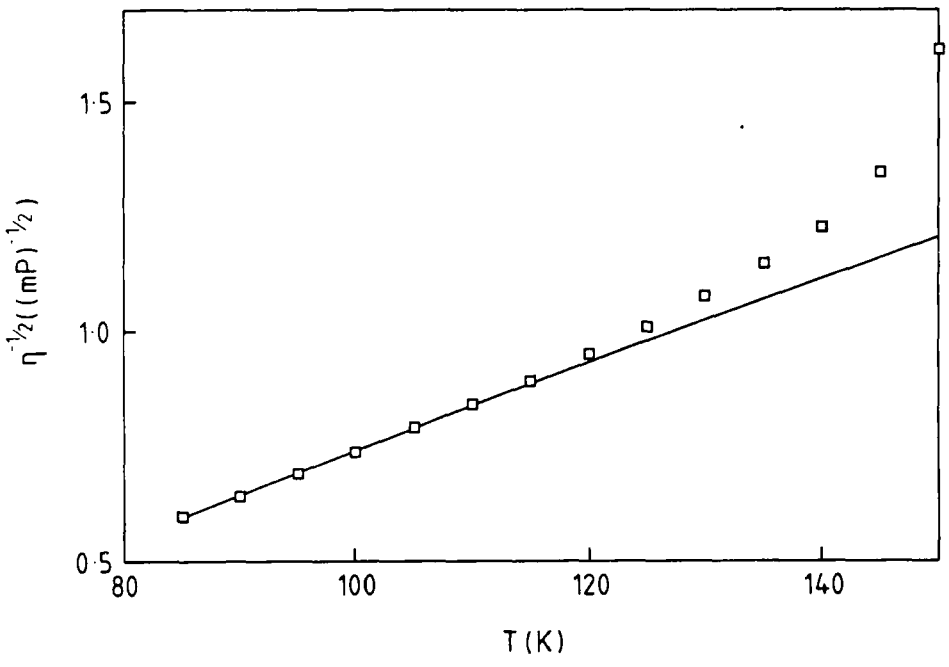


**Figure 2.3** Square root of fluidity as a function of temperature for liquid argon along the saturated vapour pressure line. The squares refer to experimental data from Haynes[21], and the line is obtained from Eq. (2.18).



made quite recently using data for argon at high densities[20]. However, for the liquid alkali metals, using the values of shear viscosity and density listed by Shpil'rain *et al.*, we find that $\sqrt{T}/\eta$, rather than the fluidity, shows an approximate linear relationship with $n^{-1}$, although over a limited temperature range only (of approximately two to three times the melting temperature). This has been noted before[34], and is consistent with the hard sphere model for the transport properties of simple liquids considered in Section 5.

Within the Arrhenius concept, the equation $D = D_0 e^{-E_D/k_B T}$, has been proposed for the temperature dependence of diffusion coefficients. This type of expression is supported by theoretical arguments based on the quasi-lattice model of a liquid, and is apparently given some credence from an examination of self-diffusion data in the liquid alkali metals[35]. Once again, the temperature range is rather limited. Nachtrieb[36] has carefully examined the way in which $D$ varies with temperature for the liquid metals indium (with two different sets of data), mercury and tin, using what he considered to be the best data available. He investigated log $D$ versus $T^{-1}$, $D$ versus $T$, $D$ versus $\sqrt{T}$ and $D$ versus $T^2$. Unfortunately, there are no universal conclusions to be drawn from the results. For tin and one set of indium data, the first two plots gave equally good straight lines. No linearity could be claimed for any of the plots with the remaining data.

The observation that the fluidity of the alkali metals depends linearly on $\sqrt{T}$ has implications for the temperature dependence of $D$. The apparent applicability in simple liquids of the Stokes-Einstein relation, $D = k_B T/4\pi\eta R$ ($R$ being an effective particle radius), suggests that $D/T$ should vary linearly with $\sqrt{T}$. This of course assumes that $R$ is independent of temperature, which will be a reasonable assumption over a limited temperature range. We have tested this prediction for liquid Na, with data at constant pressure[37]. The result is shown in Figure 2.4. The spread of the data points at nearly the same temperature gives an idea of the accuracy of the measurements. It is just as convincing as an Arrhenius plot. Unfortunately, because of the limited range of temperature a linear dependence on $T$ cannot be ruled out either. These alternatives were used to examine data obtained at constant volume by Ozelton and Swalin[7]. In this case a linear plot is not apparent for any of them.

For the inert gas liquids Ar, Kr and Xe, and also for $CH_4$, diffusion coefficient data has been approximately fitted by the Arrhenius form[38]. This was done along a number of isobars, and for argon, along the saturated vapour pressure curve as well. Here, the pressure changed from 1.32 atm. to 47 atm. We have compared the Arrhenius fit along the vapour pressure line with the simpler one of $D$ versus $T$, and find that the latter displays a more convincing linear behaviour. The result is shown in Figure 2.5. For the Arrhenius plot the points show a distinct curvature which is hard to reconcile with a random scatter within the error bars.



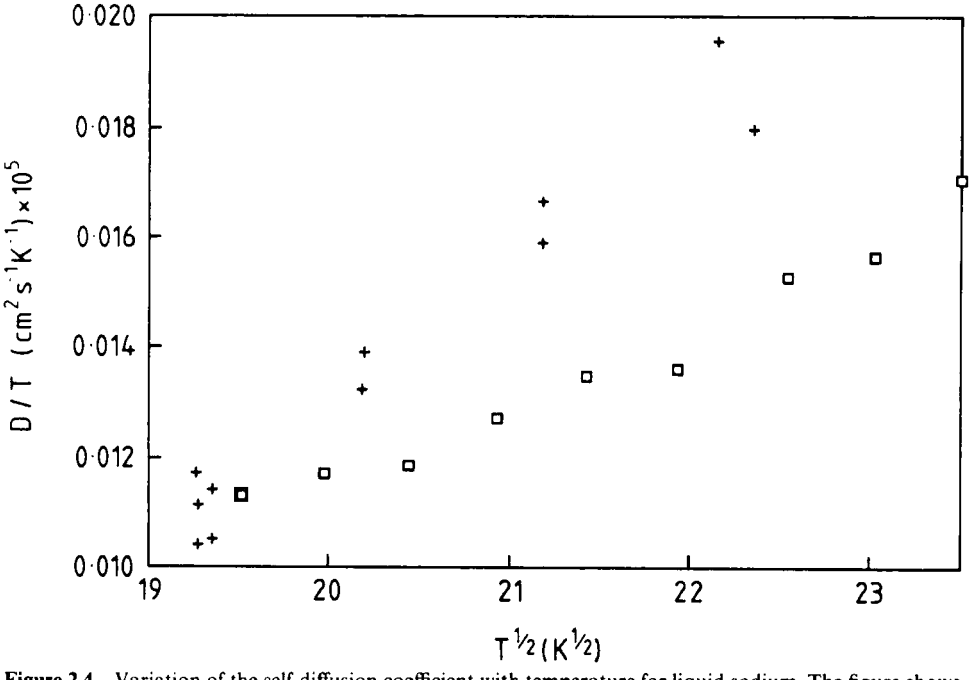


**Figure 2.4** Variation of the self-diffusion coefficient with temperature for liquid sodium. The figure shows $D/T$ versus $T^{1/2}$, the crosses denoting data at constant pressure[37], and the squares refer to constant volume measurements[7].

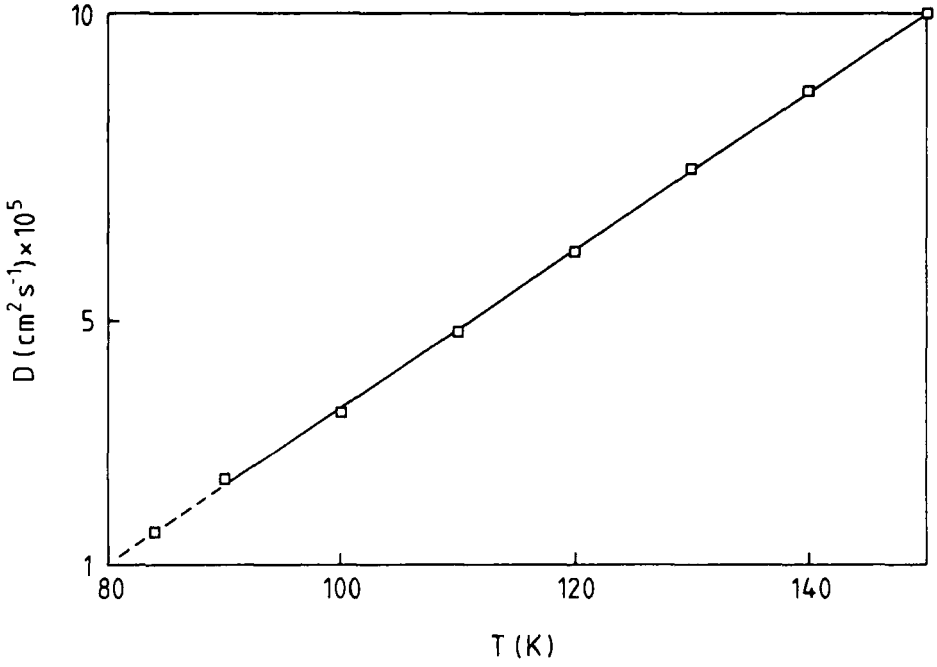


**Figure 2.5** Self-diffusion coefficient of liquid argon as a function of temperature along the saturated vapour pressure curve. Experimental data points from Nagizadeh and Rice[38], except for the lowest temperature[39,40], where we take $D = 1.53 \times 10^{-5}$ cm$^2$ s$^{-1}$. The straight line is from a least squares fit to the data of Nagizadeh and Rice.



Tyrell and Harris[6] have quite recently reviewed the topic and discussed the conceptual problems involved in the idea of diffusion occurring as a result of atoms jumping into vacancies, with the process requiring an activation energy. They also suggest that there is now some fairly direct experimental evidence that diffusion in liquids does not occur by individual molecular "leaps", although the liquid involved in the investigation cannot be classified as "simple" in the context of this review. The experiment, by Ruby *et al.*[41], concerned the diffusion of the $^{55}$Fe isotope in a *supercooled* solution of an iron salt in a glass-forming liquid. Using a Mössbauer technique to measure the broadening of the line shape of the resonant $\gamma$-rays, due to atomic motion, and assuming a jump model for diffusion, information on the average distance between jumps could be obtained. In a quasi-lattice interpretation of the diffusive mechanism, the jump distance involved would be expected to be of the order of a molecular diameter. The experiment showed that the average individual movements must be very much smaller than that, and this was interpreted as evidence in support of diffusion proceeding by a continuous series of small displacements rather than jumps. Nevertheless, the experiment has a rather puzzling feature. It has to be pointed out that the observed temperature dependence of the isotope diffusion coefficient could be fitted reasonably well by an Arrenius law, *over a range where D*

*changed by three orders of magnitude.* By itself, this would tend to suggest an activated diffusion process in the supercooled liquid. However, an equally good (and probably better) power law fit, of the type discussed by Taborek *et al.*, cannot be ruled out.

Quite recently, a systematic investigation of the thermal conductivity data for the inert gas liquids has been reported by van Loef[33]. The results are expressed in terms of the relationship of the thermal resistivity ($\lambda^{-1}$) with molar volume. Again, the variables are expressed in reduced form and he finds that $\lambda^{-1}$ varies linearly with molar volume. The temperature range extends from the triple to the critical point and, as with the fluidity, a corresponding states principle is found to operate. Two further results emerge: (i) in the liquid, $\lambda$ varies only slightly with temperature along an isochore and (ii) the thermal resistivity increases by a factor of $\approx 2$ on increasing the volume, from the triple point value, by about 30%. In the above reference the investigation of viscosity and thermal conductivity is extended to diatomic liquids and to mixtures, although this is not of principle concern here.

In the next section we review the framework of atomic transport theory, and derive exact expressions for the transport coefficients in terms of Green-Kubo integrands.



## 3 GENERAL THEORETICAL FRAMEWORK

In a discussion of the transport properties of a one-component liquid the fundamental microscopic dynamical variables are the single particle and number density fluctuations, $n_s(\mathbf{k}, t)$ and $n(\mathbf{k}, t)$ respectively, the momentum density fluctuations, $\mathbf{P}(\mathbf{k}, t)$, and the energy density fluctuations, $E(\mathbf{k}, t)$. All are conserved as $k \to 0$ and are defined as

$$n_s(\mathbf{k}, t) = \exp[i\mathbf{k} \cdot \mathbf{r}_1(t)] \quad \text{and} \quad n(\mathbf{k}, t) = \sum_j \exp[i\mathbf{k} \cdot \mathbf{r}_j(t)],$$

$$\mathbf{P}(\mathbf{k}, t) = \sum_j m\mathbf{v}_j(t) \exp[i\mathbf{k} \cdot \mathbf{r}_j(t)]$$

and

$$\begin{aligned} E(\mathbf{k}, t) &= \sum_j \tfrac{1}{2}\{mv_j^2(t) + \sum_{j' \neq j} \varphi(r_{j'j}(t)\} \exp[i\mathbf{k} \cdot \mathbf{r}_j(t)] \\ &\equiv \sum_j E_j(t) \exp[i\mathbf{k} \cdot \mathbf{r}_j(t)] \end{aligned} \tag{3.1}$$

In the following theory it will be convenient to define fluctuation variables $\hat{A}(t) = A(t) - \langle A(t) \rangle$. Note that $\langle n_s(\mathbf{k}, t) \rangle = \delta_{\mathbf{k},0}$, $\langle n(\mathbf{k}, t) \rangle = N\delta_{\mathbf{k},0}$, $\langle \mathbf{P}(\mathbf{k}, t) \rangle = 0$ and $\langle E(\mathbf{k}, t) \rangle = \langle H \rangle \delta_{\mathbf{k},0}$, where $H$ is the Hamiltonian of the system. Choosing $\mathbf{k}$ in the $z$ direction, the equations of motion are

$$\dot{n}_s(\mathbf{k}, t) = ikv_1^z(t)n_s(\mathbf{k}, t), \quad \dot{n}(\mathbf{k}, t) = (ik/m)P^z(\mathbf{k}, t),$$

with

$$\dot{P}^z(\mathbf{k}, t) = ik \sum_j \{m[v_j^z(t)]^2 - \tfrac{1}{2} \sum_{j' \neq j} [z_{j'j}(t)/r_{j'j}(t)]^2 \Phi_k(r_{j'j}(t))\} \exp[ikz_j(t)]$$

$$\dot{P}^x(\mathbf{k}, t) = ik \sum_j \{mv_j^z(t)v_j^x(t) - \tfrac{1}{2} \sum_{j' \neq j} [z_{j'j}(t)x_{j'j}(t))/r_{j'j}^2(t)]\Phi_k(r_{j'j}(t))\} \exp[ikz_j(t)]$$

$$\dot{P}^y(k, t) \quad \text{as} \quad \dot{P}^x(k, t) \quad \text{with } x \to y,$$

and

$$\dot{E}(\mathbf{k}, t) = ik \sum_j \{E_j(t)v_j^z(t) - \tfrac{1}{4} \sum_{j' \neq j} [(\mathbf{v}_{j'}(t) + \mathbf{v}_j(t)) \cdot \mathbf{r}_{j'j}(t) z_{j'j}(t)/r_{j'j}^2(t)]\Phi_k(r_{j'j}(t))\} \exp[ikz_j(t)] \tag{3.2}$$

where $\Phi_k(r) = r\varphi'(r)(1 - \exp[-ikz])(ikz)^{-1}$ with $\varphi(r)$ the pair-potential energy. The proportionality to $ik$, present in all these equations, reflects the conservation of the corresponding variable.

### 3.1 *The Generalized Langevin Equation*

A 'generalized hydrodynamics', based on microscopic quantities, can be established by means of the formally exact Mori-Zwanzig approach to microdynamics[42]. The latter makes use of projection operators, so that from any dynamical variable the part behaving like the conserved quantities is extracted. Thus the role of the variables defined in Eqs (3.1) is emphasized by the approach, establishing a connection with ordinary continuum hydrodynamics in its linearized version. However, the microscopic theory is not restricted to slowly varying fluctuations, and this results in the introduction of wavevector- and frequency-dependent transport coefficients.

To demonstrate these predictions we consider the conserved variables to be arranged as a column vector $A(\mathbf{k}, t) = \{A_i(\mathbf{k}, t)\}$. The Mori-Zwanzig approach starts from the usual equations of motion $\dot{\hat{A}}_i(\mathbf{k}, t) = iL\hat{A}_i(\mathbf{k}, t)$ where $L$ is the Liouville operator of the system. Then, by introducing projection operators defined as

$$P \cdots = \sum_{jl} \langle A_j^*(\mathbf{k}) \cdots \rangle \langle A^*(\mathbf{k})A(\mathbf{k}) \rangle_{jl}^{-1} \hat{A}_l(\mathbf{k}) \tag{3.3}$$

the time correlation function $\langle \hat{A}_j^*(\mathbf{k}, 0)\hat{A}_i(\mathbf{k}, t) \rangle$ is shown to satisfy the following generalized Langevin equation

$$\frac{d}{dt} \langle \hat{A}_j^*(\mathbf{k}, 0)\hat{A}_i(\mathbf{k}, t) \rangle = i \sum_l \Omega_{il}(\mathbf{k}) \langle \hat{A}_j^*(\mathbf{k}, 0)\hat{A}_i(\mathbf{k}, t) \rangle - \sum_l \int_0^t d\tau K_{il}(\mathbf{k}, \tau) \langle \hat{A}_j^*(\mathbf{k}, 0)\hat{A}_i(\mathbf{k}, t - \tau) \rangle \tag{3.4}$$

(Note that in the definition of the projection operator, and frequently in the subsequent discussion, we use the notation $A(\mathbf{k}, t = 0) = A(\mathbf{k})$ for any variable $A$.) In the above equation the "proper frequency matrix", $\Omega$, is defined by

$$i\Omega_{ij}(\mathbf{k}) = \sum_l \langle \hat{A}_l^*(\mathbf{k})\hat{A}_i(\mathbf{k}) \rangle \langle \hat{\mathbf{A}}^*(\mathbf{k})\hat{\mathbf{A}}(\mathbf{k}) \rangle_{lj}^{-1} \tag{3.5}$$

and the "memory matrix" $\mathbf{K}(\mathbf{k}, t)$ by

$$K_{ij}(\mathbf{k}, t) = \sum_l \langle f_l^*(\mathbf{k}) e^{i(1-P)Lt} f_i(\mathbf{k}) \rangle \langle \hat{\mathbf{A}}^*(\mathbf{k}) \hat{\mathbf{A}}(\mathbf{k}) \rangle_{lj}^{-1} \tag{3.6}$$

where the "random force" $f_i(\mathbf{k}) \equiv (1 - P)\dot{\hat{A}}_i(\mathbf{k})$ evolves in time with the anomalous propagator $e^{i(1-P)Lt}$, which makes it orthogonal at all times to the components of the set $\hat{\mathbf{A}}(\mathbf{k})$.

The conserved character of the variables $A_i(\mathbf{k})$ has two important consequences. First, the proportionality of $\dot{\hat{A}}_i(\mathbf{k})$ to $k$ implies that the non-zero elements of the proper frequency matrix are also proportional to $k$ (assuming that the elements of the susceptibility matrix $\langle \hat{\mathbf{A}}^*(\mathbf{k}) \hat{\mathbf{A}}(\mathbf{k}) \rangle$ are regular as $k \to 0$, a requirement which is well satisfied away from critical points). Moreover, the non-zero components of the random force $f_i(\mathbf{k}) \propto k$ make the elements of the memory matrix at least proportional to $k^2$. In the limit $k \to 0$, the leading order dependence $K_{il}(\mathbf{k}, t) \propto k^2$ gives rise to a further simplification. It is easily shown[43] that the replacement of the anomalous propagator $e^{i(1-P)Lt}$ with the ordinary one $e^{iLt}$ is correct to order $k$. Thus, having extracted the leading $k^2$ dependence, $K_{il}(\mathbf{k} \to 0, t)$ can be expressed in terms of an ordinary time correlation function.

Having outlined the general framework, we are now ready to discuss its predictions for the basic dynamical properties of the system.

### 3.2 *Microscopic Dynamics and Transport Coefficients*

*a) Single particle motion: the self-diffusion coefficient* The correlations involving the single particle density $n_s(\mathbf{k}, t)$ are a factor $(1/N)$ smaller than those involving $n(\mathbf{k}, t)$. Thus, $n_s(\mathbf{k}, t)$ can be considered to be effectively uncoupled from the other variables, and the Mori-Zwanzig matrix formulation reduces to a scalar one. The equation for the self time correlation function $F_s(k, t) = \langle \hat{n}_s^*(\mathbf{k}, 0) \hat{n}_s(\mathbf{k}, t) \rangle$ becomes

$$\dot{F}_s(k, t) = -\int_0^t d\tau \, K_s(k, \tau) F_s(k, t - \tau) \tag{3.7}$$

since the proper frequency $i\Omega_s(\mathbf{k}) = \langle \hat{n}_s^*(\mathbf{k}) \dot{\hat{n}}_s(\mathbf{k}) \rangle$ vanishes because of the opposite symmetries of $n_s$ and $\dot{n}_s$ under time reversal. The memory function reads

$$K_s(k, t) = k^2 \langle v_1^z(0) \exp[-ikz_1(0)] e^{i(1-P_s)Lt} v_1^z(0) \exp[ikz_1(0)] \rangle \tag{3.8}$$

where $P_s$ denotes the projection operator onto the variable $\hat{n}_s(\mathbf{k})$. A formal solution of Eq. (3.7) is obtained by introducing Laplace transforms $\tilde{F}(z) = \int_0^\infty dt \exp[-zt] F(t)$, so that

$$\tilde{F}_s(z) = [z + k^2 \tilde{D}(k, z)]^{-1} \tag{3.9}$$

where

$$\begin{aligned} \tilde{D}(k, z) &\equiv \tilde{K}_s(k, z)/k^2 \\ &= \int_0^\infty dt \, e^{-zt} \langle v_1^z \exp[-ikz_1] e^{i(1-P_s)Lt} v_1^z \exp[ikz_1] \rangle \end{aligned} \tag{3.10}$$

The usual Fourier spectrum of $F_s(k, t)$ is $S_s(k, \omega) = (1/\pi)\,\mathrm{Re}\,\tilde{F}(z = i\omega)$, and can be determined experimentally from the incoherent part of the inelastic neutron scattering cross-section.

As a general remark, the microscopic equivalent of the "local equilibrium" assumption introduced in ordinary continuum hydrodynamics requires the consideration of fluctuations with wavelengths much larger than the mean free path. Moreover, the behaviour of the relevant correlations is explored at times sufficiently large that many interactions have actually occurred. In such a "hydrodynamic regime" where $k \to 0$ and $\omega \to 0$ (in that order) all the microscopic details are hidden in a few constants, which are essentially the ordinary transport coefficients.

In the case of single particle motion, the relevant property is self-diffusion. The corresponding *diffusion coefficient* in the hydrodynamic regime is

$$D = \lim_{z \to 0} \lim_{k \to 0} \tilde{D}(k, z) = \int_0^\infty dt \langle v_1^z(0) v_1^z(t) \rangle = \tfrac{1}{3} \int_0^\infty dt \langle \mathbf{v}_1(0) \cdot \mathbf{v}_1(t) \rangle \tag{3.11}$$

This equation relates an ordinary transport coefficient to the time integral of an autocorrelation function[44,45]. Other examples of a "Green-Kubo relation" will subsequently appear. In this particular case, Eqs (3.9), (3.10) and (3.11) imply that $F_s(k, t) = \exp(-Dk^2 t)$ in the hydrodynamic limit, which has the slow decay so typical of this regime.

More generally, outside the hydrodynamic regime, Eq. (3.10) may be used to define a complex wavevector- and frequency-dependent diffusion coefficient $\tilde{D}(k, z = i\omega)$. Even if the presence of the anomalous propagator in the definition of $\tilde{D}(k, z)$ complicates the theoretical analysis, it is often possible to gain some insight into the features of $F_s(k, t)$ by making simple ansätze for the time dependence of $D(k, t)$ (e.g. gaussian or exponential), with the constraint that certain sum rules derived from the short-time dynamics must be satisfied. A less phenomenological approach is based on kinetic and/or mode-coupling arguments; an example of the latter will be briefly discussed in Section 6.

*b) Transverse momentum current: the shear viscosity coefficient.* The overall isotropy of the system leads to another simplification in the remaining collective variables, namely the decoupling of the momentum density variables perpendicular to $\mathbf{k}$, $P^x(\mathbf{k}, t)$ and $P^z(\mathbf{k}, t)$, from the other variables. Since there is no cross correlation between these two, equivalent, components we are again left with a single variable, say $P^x(\mathbf{k}, t)$. The transverse current correlation function $C_T(k, t) = \langle [P^x(\mathbf{k}, 0)]^* P^x(\mathbf{k}, t) \rangle$ has the equation of motion

$$\dot{C}_T(k, t) = -\int_0^t dt K_T(k, \tau) C_T(k, t - \tau) \tag{3.12}$$

where, again, the proper frequency vanishes. Noting that $C_T(k, t = 0) = Nmk_B T$, the memory function reads

$$K_T(k, t) = (k^2/Nmk_B T) \langle [\sigma^{zx}(\mathbf{k})]^* e^{i(1 - P_T)Lt} \sigma^{zx}(\mathbf{k}) \rangle \tag{3.13}$$

with $P_T$ the operator which projects onto $P^x(\mathbf{k})$, and

$$\sigma^{\alpha\beta}(\mathbf{k}) = \sum_j \{mv_j^\alpha v_j^\beta - \tfrac{1}{2} \sum_{j' \neq j} (r_{j'j}^\alpha r_{j'j}^\beta / r_{j'j}^2) \Phi_k(r_{j'j})\} \exp[ikz_j] \tag{3.14}$$

is the microscopic expression of the $(\alpha, \beta)$ element of the stress tensor. The formal solution of Eq. (3.12) in terms of Laplace transforms reads

$$\tilde{C}_T(k, z) = Nmk_B T[z + (k^2/nm)\tilde{\eta}(k, z)]^{-1} \tag{3.15}$$

where

$$\begin{aligned} \tilde{\eta}(k, z) &= (nm/k^2)\tilde{K}_T(k, z) \\ &= (1/Vk_B T) \int_0^\infty dt e^{-zt} \langle [\sigma^{zx}(\mathbf{k})]^* e^{i(1-P_T)Lt} \sigma^{zx}(\mathbf{k}) \rangle \end{aligned} \tag{3.16}$$

In the hydrodynamic limit $k \to 0$, $z \to 0$ we may ignore $P_T$ in the time propagator, obtaining

$$\eta = \lim_{z \to 0} \lim_{k \to 0} \tilde{\eta}(k, z) = (1/Vk_B T) \int_0^\infty dt \langle \sigma^{zx}(\mathbf{k} = 0, 0) \sigma^{zx}(\mathbf{k} = 0, t) \rangle \tag{3.17}$$

where

$$\sigma^{zx} \equiv \sigma^{zx}(\mathbf{k} = 0) = \sum_j \{mv_j^z v_j^x - \tfrac{1}{2} \sum_{j' \neq j} (z_{j'j} x_{j'j} / r_{j'j}) \varphi'(r_{j'j})\} \tag{3.18}$$

The result (3.17) is the Green-Kubo relation for the *shear viscosity coefficient*. The corresponding Green-Kubo integrand

$$\eta(t) = (1/Vk_B T) \langle \sigma^{zx}(0) \sigma^{zx}(t) \rangle \tag{3.19}$$

is the autocorrelation function of the non-diagonal components of the stress tensor, and is usually referred to as the stress autocorrelation function. From the expression for $\sigma^{zx}$ in Eq. (3.18) it is readily seen that $\eta(t)$ is made up of a purely kinetic contribution, a purely potential contribution and a part involving cross terms. While at low densities the kinetic part is dominant, in a liquid the value of $\eta$ is almost totally determined by the potential energy contribution, given by

$$\begin{aligned} \eta_{pp}(t) = (\tfrac{1}{4} Vk_B T) \langle & \sum_{j'j(j' \neq j)} [z_{j'j}(0) x_{j'j}(0) / r_{j'j}(0)] \varphi'(r_{j'j}(0)) \cdot \\ & \cdot \sum_{l'l(l' \neq l)} [z_{l'l}(t) x_{l'l}(t) / r_{l'l}(t)] \varphi'(r_{l'l}(t)) \rangle \end{aligned} \tag{3.20}$$

In contrast with the case of diffusion, the Green-Kubo integrand for the shear viscosity is a collective quantity which involves up to four distinct particles. This complicated structure is simplified only at $t = 0$, where, for example, the exact hierarchies for the three- and four-body distribution functions can be exploited to reduce $\eta(0)$ to an expression involving only two distinct particles. By this means we

obtain a result for $\eta(0)$ (which coincides with the rigidity modulus, $G$, of the liquid) given by

$$\eta(0) = nk_B T + (n^2/2) \int d\mathbf{r} z^2 \frac{\partial^2 \varphi(r)}{\partial x^2} g(r) \tag{3.21}$$

with $g(r)$ the radial distribution function.

In the hydrodynamic regime the transverse current correlation function $C_T(k, t) = C_T(k, t = 0)\exp[-(k^2/nm)\eta t]$ shows a slow monotonous decay with no trace of propagating transverse modes. In analogy with the discussion of single particle motion we may define a generalized viscosity coefficient, $\tilde{\eta}(k, z = i\omega)$, by means of Eq. (3.16). Again, exact analysis is difficult, but a simple "viscoelastic" ansatz like $\eta(k, t) = \eta(k, 0)\exp[-t/\tau(k)]$ (followed by reasonable assumptions about the $k$-dependence of $\tau(k)$[46]) is sufficient to demonstrate that underdamped transverse modes may be supported by the liquid at larger $k$. Fortunately, this occurs in a wavevector range which is readily accessible in computer simulation experiments.



*c) Density fluctuations: thermal conductivity and the longitudinal viscosity coefficient* The fluctuations of the remaining three conserved variables, $n(\mathbf{k}, t)$, $P^z(\mathbf{k}, t)$ and $E(\mathbf{k}, t)$ are coupled together and must be treated simultaneously in the Mori-Zwanzig framework. The complications in the matrix algebra are partially eliminated by replacing $E(\mathbf{k}, t)$ with the new conserved variables[47,48]

$$\hat{\varepsilon}(\mathbf{k}, t) = \hat{E}(\mathbf{k}, t) - \langle \hat{n}(-\mathbf{k})\hat{E}(\mathbf{k})\rangle [\langle \hat{n}(-\mathbf{k})\hat{n}(\mathbf{k})\rangle]^{-1} \hat{n}(\mathbf{k}, t) \tag{3.22}$$

The new set $\{\hat{A}_1(\mathbf{k}), \hat{A}_2(\mathbf{k}), \hat{A}_3(\mathbf{k})\} = \{\hat{n}(\mathbf{k}), \hat{P}^z(\mathbf{k}), \hat{\varepsilon}(\mathbf{k})\}$ consists of mutually orthogonal variables, and the susceptibility matrix $\langle \hat{A}(\mathbf{k})^* \hat{A}(\mathbf{k})\rangle$, together with its inverse, is diagonal.

The proper frequency matrix $\Omega(\mathbf{k})$ (Eq. (3.5)) comprises only non-diagonal elements because of time-reversal symmetry. In particular

$$\begin{aligned} &\Omega_{12}(k) = k/m, \quad \Omega_{21}(k) = (k/S(k))k_B T, \quad \Omega_{13}(k) = \Omega_{31}(k) = 0 \\ &\Omega_{23}(k) = (k/\langle \hat{\varepsilon}(-\mathbf{k})\hat{\varepsilon}(\mathbf{k})\rangle)B(k) \quad \text{and} \quad \Omega_{32}(k) = (k/Nmk_B T)B(k) \end{aligned} \tag{3.23}$$

where we have written $\langle \hat{n}(-\mathbf{k})\hat{n}(\mathbf{k})\rangle = NS(k)$ ($S(k)$ being the static structure factor of the liquid), and introduced the quantity

$$B(k) \equiv \langle \hat{E}(\mathbf{k})^* \sigma^{zz}(\mathbf{k})\rangle - (k_B T/S(k))\langle \hat{n}(-k)\hat{E}(\mathbf{k})\rangle \tag{3.24}$$

Note that according to the virial theorem $\langle \sigma^{zz}(\mathbf{k})\rangle = PV\delta_{\mathbf{k},0}$ with $P$ the system's pressure.

The memory matrix elements $K_{ii}(\mathbf{k}, t)$ involve correlations between the components $f_i(\mathbf{k}) = (1 - P_0)\dot{\hat{A}}_i(\mathbf{k})$, where $P_0$ projects onto the set $\{\hat{A}_i(\mathbf{k})\}$ ($i = 1, 2, 3$). From the equations of motion, written in the form

$$\dot{\hat{n}}(\mathbf{k}, t) = (ik/m)P^z(\mathbf{k}, t), \dot{\hat{P}}^z(\mathbf{k}, t) = ik\sigma^{zz}(\mathbf{k}, t) \quad \text{and} \quad \dot{\hat{E}}(\mathbf{k}, t) = ikq^z(\mathbf{k}, t) \tag{3.25}$$

in which $q^z(\mathbf{k}, t)$ is the $z$-component of the energy current, it is easily seen that

$$f_1(\mathbf{k}) = 0$$

$$f_2(\mathbf{k}) = ik\{\sigma^{zz}(\mathbf{k}) - (k_B T/S(k))\hat{n}(\mathbf{k}) - (B(k)/\langle\hat{\varepsilon}(-\mathbf{k})\hat{\varepsilon}(\mathbf{k})\rangle)\hat{\varepsilon}(\mathbf{k})\} \equiv ik\sigma'^{zz}(\mathbf{k})$$

and

$$f_3(\mathbf{k}) = ik\{q^z(\mathbf{k}) - (1/Nmk_B T)B(k)P^z(\mathbf{k})\} \equiv ikq'^z(\mathbf{k}) \tag{3.26}$$

Consequently the non zero elements of the memory matrix read

$$\tilde{K}_{22}(\mathbf{k}, z) = (k^2/Nmk_B T)\int_0^\infty dt e^{-zt}[\sigma'^{zz}(\mathbf{k})]^* e^{i(1-P_0)Lt}\sigma'^{zz}(\mathbf{k})$$

$$\tilde{K}_{33}(\mathbf{k}, z) = (k^2/\langle\hat{\varepsilon}(-\mathbf{k})\hat{\varepsilon}(\mathbf{k})\rangle\int_0^\infty dt e^{-zt}\langle[q'^z(\mathbf{k})]^* e^{i(1-P_0)Lt}q'^z(\mathbf{k})\rangle$$

$$\tilde{K}_{23}(\mathbf{k}, z) = (k^2/\langle\hat{\varepsilon}(-\mathbf{k})\hat{\varepsilon}(\mathbf{k})\rangle)\int_0^\infty dt e^{-zt}\langle[q'^z(\mathbf{k})]^* e^{i(1-P_0)Lt}\sigma'^{zz}(\mathbf{k})\rangle$$

$$\tilde{K}_{32}(\mathbf{k}, z) = (k^2/Nmk_B T)\int_0^\infty dt e^{-zt}\langle[\sigma'^{zz}(\mathbf{k})]^* e^{i(1-P_0)Lt}q'^z(\mathbf{k})\rangle \tag{3.27}$$

We now have the information to write down a set of Mori equations for the dynamic correlations $\langle\hat{A}_j^*(\mathbf{k}, 0)\hat{A}_i(\mathbf{k}, t)\rangle$ $(i, j = 1, 2, 3)$. The most interesting case is $\langle\hat{A}_1^*(\mathbf{k}, 0)\hat{A}_1(\mathbf{k}, t)\rangle = \langle\hat{n}(-\mathbf{k}, 0)\hat{n}(\mathbf{k}, t)\rangle = NF(k, t)$, where $F(k, t)$ is the intermediate scattering function. The spectrum $S(k, \omega)$ of this density fluctuation correlation function is directly observed in light scattering experiments on fluids as well as in measurements of the coherent part of the neutron inelastic scattering cross section. The formal solution is readily obtained by Laplace transform, and reads

$$\frac{\tilde{F}(k, z)}{S(k)} =$$

$$\left(z + \frac{k^2[k_B T/mS(0)]}{z + \tilde{K}_{22}(\mathbf{k}, z) + [i\Omega_{23}(\mathbf{k}) - \tilde{K}_{23}(\mathbf{k}, z)][i\Omega_{32}(\mathbf{k}) - \tilde{K}_{32}(\mathbf{k}, z)][z + \tilde{K}_{33}(\mathbf{k}, z)]}\right)^{-1} \tag{3.28}$$

In the hydrodynamic regime we may now apply the limiting procedures discussed previously: extraction of the leading wavevector dependencies ($k$ in the proper frequencies, $k^2$ in the memory functions), replacement of $e^{i(1-P_0)Lt}$ with $e^{iLt}$ in the memory functions, and finally evaluation for $z = 0$. Using isotropy arguments, the quantities $\tilde{K}_{23}$ and $\tilde{K}_{32}$ are shown to give no contribution to order $k^2$. To order $k$, because the memory functions are zero, $S(k, \omega)$ is characterized by three $\delta$-like peaks at the frequencies

$$\omega = 0 \quad \text{and} \quad \omega(k) = \pm k[(k_B T/mS(0)) + (B^2(k=0)/Nmk_B T\langle\hat{\varepsilon}(0)\hat{\varepsilon}(0)\rangle]^{1/2} \tag{3.29}$$

Noting that $S(0) = nk_B T\chi_T$ (where $\chi_T$ is the isothermal compressibility) and also that $\langle\hat{\varepsilon}(0)\hat{\varepsilon}(0)\rangle = \langle\hat{H}\hat{H}\rangle = Nk_B T^2 c_v$ (where $c_v$ is the specific heat per particle at constant volume), it is possible to show that

$$B^2(k=0)/\langle\hat{\varepsilon}(0)\hat{\varepsilon}(0)\rangle = (N(k_B T)^2/S(0))T[V^{-1}\partial V/\partial T]^2/nc_v\chi_T$$
$$= (N(k_B T)^2/S(0))(c_p - c_v)/c_v \tag{3.30}$$

with $c_p = \gamma c_v$, the specific heat at constant pressure. To obtain this result we have evaluated

$$\langle E(k=0)\sigma^{zz}(\mathbf{k}=0)\rangle = k_B T^2(\partial\langle\sigma^{zz}(\mathbf{k}=0)/\partial T)_v = k_B T^2 V(\partial P/\partial T)_V$$
$$= k_B T^2(N/n\chi_T)V^{-1}(\partial V/\partial T)_P \tag{3.31}$$

and used a well known thermodynamic relation for the difference $c_p - c_v$. The final result $\omega(k) = \pm k[\gamma k_B T/ms(0)]^{1/2} = \pm kc_s$ coincides with the frequencies of the Brillouin doublet, well known from continuum hydrodynamics, $c_s$ being the sound velocity.

At the order $k^2$, the non-vanishing memory functions $\tilde{K}_{22}$ and $\tilde{K}_{33}$ provide decay mechanisms for the Rayleigh–Brillouin triplet, so that Eqs. (3.29) become

$$\omega = ik^2(\lambda/\gamma nc_V) \quad \text{and} \quad \omega(k) = \pm kc_s - ik^2\Gamma \tag{3.32}$$

In these expressions $\lambda$ is the *thermal conductivity* and $\Gamma = \frac{1}{2}[(\lambda/\gamma nc_v)(\gamma - 1) + \eta_L/nm]$ is related to the sound attenuation coefficient, with $\eta_L$ the *longitudinal viscosity coefficient*. It is readily shown that $\lambda$ is obtained as

$$\lambda = (c_v/n)(\tilde{K}_{33}(\mathbf{k}\to 0, z=0)/k^2) = (1/Vk_BT^2)\int_0^\infty dt\langle q^z(\mathbf{k}=0,0)q^z(k=0,t)\rangle \tag{3.33}$$

Comparison with the second of Eqs (3.27) shows that $q'^z(\mathbf{k}=0)$ has been replaced by

$$q^z(\mathbf{k}=0) = \sum_j \{E_j v_j^z - \tfrac{1}{4}\sum_{j'\neq j}(\mathbf{v}_{j'} + \mathbf{v}_j)\cdot \mathbf{r}_{j'j} z_{j'j}/r_{j'j}\varphi'(r_{j'j})\} \tag{3.34}$$

since the difference between the two quantities is proportional to $P^z(\mathbf{k}=0) = \sum_j mv_j^z$, which can always be made to vanish at all times by a suitable choice of reference frame.

Finally the longitudinal viscosity is defined in terms of the memory function $\tilde{K}_{22}(k,z)$ by the relation

$$\eta_L = (nm/k^2)\tilde{K}_{22}(\mathbf{k}\to 0, z=0) = (1/Vk_BT)\int_0^\infty dt\langle\sigma'^{zz}(\mathbf{k}=0,0)\sigma'^{zz}(\mathbf{k}=0,t)\rangle \tag{3.35}$$

which is the "diagonal" counterpart of the result (3.17) for the shear viscosity coefficient; in the longitudinal case the appearance of $\sigma'^{zz}$ instead of the usual stress tensor component $\sigma^{zz}$ is responsible for the presence of additional terms in the Green–Kubo integrand (3.35) whose significance depends on which statistical ensemble is used to evaluate the averages[4,5]. Starting from the general "viscosity tensor"

$$\eta_{\alpha\beta\gamma\delta} \equiv (1/Vk_BT)\int_0^\infty dt\langle\sigma'^{\alpha\beta}(\mathbf{k}=0,0)\sigma'^{\gamma\delta}(\mathbf{k}=0,t)\rangle \tag{3.36}$$

and exploiting all its possible symmetry properties is an isotropic system (in a way analogous to the one used for the elastic constants in continuous media), it can be demonstrated that the longitudinal viscosity may be expressed in the form

$$\eta_L = (4\eta/3) + \eta_B \tag{3.37}$$

which defines the *bulk viscosity coefficient*. The Green–Kubo result for the latter follows and is given by

$$\eta_B = (\tfrac{1}{9}Vk_BT)\sum_{\lambda,\mu}\int_0^\infty dt\langle\sigma'^{\lambda\lambda}(\mathbf{k}=0,0)\sigma'^{\mu\mu}(\mathbf{k}=0,t)\rangle \tag{3.38}$$

where the summations over $\lambda$, $\mu$ run over the cartesian components $x$, $y$, $z$.

To close this section, we shall make some further comments in connection with the generalized wavevector- and frequency-dependent transport coefficients. As previously discussed, they can be formally defined through the Mori-Zwanzig framework, where they are essentially proportional to a memory function, $\tilde{K}(k, z = i\omega)$, divided by $k^2$. Through these we can introduce purely wavevector-dependent quantities e.g. $\eta(k) \equiv \tilde{\eta}(\mathbf{k}, z = 0)$, as well as purely frequency-dependent coefficients e.g. $\eta(\omega) \equiv \tilde{\eta}(\mathbf{k} = 0, z = i\omega)$. It is important to note, however, that whereas the latter still retain the typical Green-Kubo form involving a Fourier-Laplace transform of an ordinary time autocorrelation function, the former do not, except in the $k \to 0$ limit[49]. This "asymmetric" behaviour derives from the fact that the anomalous propagator in the memory function can be replaced by the ordinary one, $e^{iLt}$, only when $k \to 0$, and this leads to a usual type of correlation function.

The framework presented above has formed the basis of much theoretical effort to understand the microdynamic behaviour and transport properties of liquids. In addition, it has been used extensively in computer simulation studies, along with alternative non-equilibrium molecular dynamic techniques. This type of approach to liquid state physics will now be discussed.



## 4 COMPUTER SIMULATION EXPERIMENTS

The first report of an extended calculation of the transport coefficients, is the paper by Alder *et al.*[50], which is the eighth of a series devoted to the properties of a hard sphere system at different thermodynamic states. The aim of the paper was "to gain insight into the nature of many-body correlations" which are fully taken into account by computer simulation. Attention was therefore focussed on the deviation of the evaluated transport coefficients from the corresponding values predicted by Enskog theory. The results are reported in Section 5, and form the basis of attempts to develop hard sphere models for the transport properties of liquids. We begin this section with a brief review of the techniques required for the calculation of transport coefficients in the rigid sphere system.

### *4.1 The Hard Sphere Fluid*

Due to the impulsive nature of the interaction between hard spheres, Green-Kubo integrands are more difficult to use directly when the generalized 'flux' involved contains the forces between particles. The calculation of the shear viscosity, for instance, cannot be performed through the direct evaluation of the Green-Kubo expression given in Eq. (3.17), i.e.

$$\eta = \int_0^\infty dt\eta(t) = (1/Vk_BT)\int_0^\infty dt\langle\sigma^{zx}(0)\sigma^{zx}(t)\rangle \tag{4.1}$$

where we may write the off-diagonal element of the stress tensor as

$$\sigma^{zx}(t) = \sum_j \{mv_j^z(t)v_j^x(t) + r_j^z(t)F_j^x(t)\} \tag{4.2}$$

with $\mathbf{F}_j(t)$ the force on sphere $j$ due to its interaction with the other spheres. To circumvent this difficulty, one makes use of the fact that Eq. (4.1) can be recast in a form similar to that used to define the diffusion coefficient through the single particle mean square displacement i.e.

$$\eta = \lim_{t\to\infty}(1/Vk_BT)(2t)^{-1}\left\langle\left[\sum_j\{mv_j^z(t)r_j^x(t) - mv_j^z(0)r_j^x(0)\}\right]^2\right\rangle \tag{4.3}$$

In practice, it turns out to be more convenient to use an expression in which only relative positions and velocities appear; this is accomplished by writing

$$\left[\sum_j mv_j^z(t)r_j^x(t)\right] - \left[\sum_j mv_j^z(0)r_j^x(0)\right] \equiv G(t) - G(0) = \int_0^t d\tau\dot{G}(\tau)$$

$$= \sum_{\text{coll}}\left[\sum_j mv_j^z(\tau_c)v_j^x(\tau_c)\right]\tau_c + \sum_{\text{coll}}\left[\sum_j m\Delta v_j^z(\tau_c)r_{ji}^x(\tau_c)\right] \tag{4.4}$$

where the sum is over all the collisions which occur in time $t$, $\tau_c$ represents the time between two successive collisions and $m\Delta v_j^z$ is the change in momentum of particle $j$ due to a collision with $i$. Note that in the last line of Eq. (4.4) the first term is purely kinetic, whereas the second represents the potential contribution.

Similar expressions can be derived for the thermal conductivity and the longitudinal viscosity i.e.

$$\lambda = \lim_{t\to\infty}(1/Vk_BT)(2t)^{-1}\left\langle\left[\sum_j\{mr_j^x(t)E_j(t) - mr_j^x(0)E_j(0)\}\right]^2\right\rangle \tag{4.5}$$

and

$$\eta_L = \lim_{t\to\infty}(1/Vk_BT)(2t)^{-1}\left\langle\left[\sum_j\{mv_j^x(t)r_j^x(t) - mv_j^x(0)r_j^x(0) - PVt\}\right]^2\right\rangle \tag{4.6}$$

As in the previous Section, $E_j$ refers to the total energy of particle $j$ and $P$ the pressure of the system. It is worth noticing that the corresponding expression for the self-diffusion coefficient $D$, reads

$$D = \lim_{t\to\infty}\tfrac{1}{3}(2t)^{-1}\langle[\mathbf{r}_1(t) - \mathbf{r}_1(0)]^2\rangle$$

$$= \lim_{t\to\infty}\tfrac{1}{3}N(2t)^{-1}\sum_j\langle[\mathbf{r}_j(t) - \mathbf{r}_j(0)]^2\rangle \tag{4.7}$$

This indicates that the statistics in this single particle case is greatly improved when compared to those of the above 'collective' coefficients. Because, in addition to the average process over the initial time $t = 0$, an extra average is performed over the individual particles of the system.

It is also possible to learn something about the physical processes which determine the value of a transport coefficient by obtaining the details of the Green-Kubo integrand. This is illustrated for the shear viscosity, for which, using Eqs (4.1), (4.3) and (4.4) it can be seen that with an appropriate definition of $G(t)$

$$\eta(t) = \langle\dot{G}(t)\dot{G}(0)\rangle = \tfrac{1}{2}(d^2/dt^2)\langle[G(t) - G(0)]^2\rangle \tag{4.8}$$

which enables the stress autocorrelation function to be derived by numerical differentiation. A similar procedure leads to the other Green-Kubo integrands. The results have been used to check the validity of Enskog theory, which predicts exponentially decaying autocorrelation functions.

The main conclusions that can be drawn from this first detailed analysis of the transport properties of a hard sphere fluid are the following:

i) The diffusion coefficient can vary significantly from Enskog theory predictions. Vortex effects[51] develop at intermediate densities and produce a pattern of neighbours which tend to maintain the motion of a given particle in its initial direction. As a result the computed value of $D$ *exceeds* the Enskog prediction. At higher densities, a particle is, on average, back-scattered so that the velocity autocorrelation function develops a negative part, which is not accounted for within Enskog theory. The vortex argument still applies but is masked by the back-scattering effect. This makes $D$ *smaller* than its Enskog value. The presence of a long-time (i.e. $t^{-3/2}$) tail in the Green-Kubo integrand has a minor effect on $D$ at liquid densities.

It should be noted also that an important dependence of the velocity autocorrelation function on the number of particles was found. The effect was explained in terms of the vortex flow induced in the finite sample. A second size-dependence, arising from the conservation of momentum requirement in the molecular dynamics calculation, is discussed and a correction applied.



ii) The same arguments apply to the kinetic part of the shear viscosity. However, at high densities the kinetic part is unimportant when compared to the potential contribution. In addition, when calculating the shear viscosity, it is particularly important to achieve an accurate evaluation of the stress autocorrelation function at intermediate and long times. (This has since been stressed by Erpenbeck and Wood[52]. Indeed, by carefully accounting for the long-time tail, and including size-dependent effects, they claim that at a packing fraction of 0.46 the shear viscosity coefficient is some 16% higher than that obtained by Alder *et al.*[50].)

iii) When compared to the stress autocorrelation function, the Green-Kubo integrands which determine the thermal conductivity and bulk viscosity show a faster time decay. In both cases, values for the coefficients were found to be close to the Enskog predictions over the range of densities explored. However, the accuracy for the bulk viscosity calculation was somewhat poorer than for the other coefficients (and a particularly large deviation from the theory was reported at the highest packing fraction considered). The relevant results are summarized in the Table 5.1.

### *4.2 Lennard-Jones Fluids*

Rahman[53] developed the simulation method to provide a more realistic description of a liquid. He was the first to report molecular dynamics results for a transport coefficient in a model in which the (864) particles interacted via a continuous two-body potential. The latter was of the Lennard-Jones type, i.e.

$$\varphi(r) = 4\varepsilon[(\sigma/r)^{12} - (\sigma/r)^{6}] \tag{4.9}$$

with parameters $\varepsilon/k_B = 120\,\mathrm{K}$ and $\sigma = 3.405\,\text{Å}$ chosen to simulate the properties of liquid argon. The self-diffusion coefficient was evaluated from the slope of a single particle mean square displacement, and with $T = 94.4\,\mathrm{K}$ (i.e. reduced temperature $T^* \equiv k_B T/\varepsilon = 0.787$) and $nm = 1.374\,\mathrm{g\,cm^{-3}}$ (i.e. reduced density $n^* \equiv n\sigma^3 = 0.807$), the value for $D = 2.43 \times 10^{-5}\,\mathrm{cm^2\,s^{-1}}$ compares favorably with the experimental result $D = 2.43 \times 10^{-5}\,\mathrm{cm^2\,s^{-1}}$ at the same density and $T = 90\,\mathrm{K}$[38]. A preliminary result at a higher temperature $T = 130\,\mathrm{K}$ and lower density $\mathrm{nm} = 1.16\,\mathrm{g\,cm^{-3}}$ suggested, however, that the temperature dependence of the diffusion coefficient was not very well reproduced by the LJ model.

Since then, extensive calculations of the diffusion coefficient in a wide range of temperatures and densities have been reported by Levesque and Verlet[54], who fitted the molecular dynamics data (see table 1 of this ref.), with an empirical formula

$$D^* = 0.006423T^*/(n^*)^2 + 0.0222 - 0.0280n^* \tag{4.10}$$

$D^*$ is the reduced value of $D$, $\sigma$ and $(m\sigma^2/48\varepsilon)^{1/2}$ being the length and time units respectively. This expression represents the data quite well except at low density ($n^* < 0.65$) and very low temperatures. For the relevant conditions the first term in Eq. (4.10) represents $\approx 90\%$ of the total, and it predicts that $D$ varies linearly with $T$, along an isochore.

However, the situation in "computer experiments" can be as confusing as that arising from real diffusion experiments. Tanaka[55] has studied the diffusion coefficient for the argon model, along the saturated vapour pressure curve. For the first state point examined by Rahman, he finds $D = 2.09 \times 10^{-5}\,\mathrm{cm^2\,s^{-1}}$ and that the temperature-dependence is best represented by the Arrhenius formula

$$D = 2.83 \times 10^{-4} \exp(-768.4/RT)\,\mathrm{cm^2\,s^{-1}} \tag{4.11}$$

$R$ being the gas constant.

More recently, Heyes has claimed that simulation diffusion data is more accurately represented, over a wider range of thermodynamic states, by an expression of the form[56]

$$D^* = a + bT^* + (c + d(T^*)^{1/4})/(n^*)^2 + (e + f(T^*)^{1/4})/n^* + n^*(g + h(T^*)^{1/4}) \tag{4.12}$$

The values for the parameters $a, \ldots, h$, are reported in Table 3 of Ref. 56.

The shear viscosity coefficient of a LJ system, for a state near the triple point, was first reported by Levesque *et al.*[57]. The value was about 30% higher than the experimental result for liquid argon. A calculation of the viscosity at the same state point has been repeated a number of times, using the same or different techniques, giving a result in close agreement with experiment. Schoen and Hoheisel[58] discuss the discrepancy with the earlier result, and conclude that the latter was incorrect. It has been argued that the cause may have been the presence of long-lived metastable states, because the system was near the solidification. Special attention has to be paid to avoiding these because they prevent a correct statistical averaging process during the molecular dynamics simulation[59].

Computer data for $\eta$ for other states of the LJ fluid are reported in Ref. 58, and the dependence of the results on the number of particles included in the simulation carefully investigated. Schoen and Hoheisel find that at the triple point, the results for

the stress autocorrelation function show no significant differences when $N \geq 500$. In addition, the very long runs performed (100,000 standard time steps) allows a precise evaluation of the Green-Kubo integrand and an accurate study of its decay at relatively long times. They conclude that after about 2.5 ps the autocorrelation function is effectively zero. This is emphasized by the following details: i) the initial, steeply decaying, part of integrand contributes more than 80% of the total value of the shear viscosity, and ii) inclusion of the subsequent contribution between 0.6 and 1.4 ps accounts for 95%. At the triple point $\eta = 2.86$ mP, in good agreement with the experimental value for argon. At state points away from the triple point, the stress autocorrelation function falls off rapidly with time and reliable values for $\eta$ can be obtained with only moderately long computer runs. There is the additional bonus that there appears to be no significant dependence of the computed value of the transport coefficient on the size of the system.

There have been fewer calculations of the bulk viscosity and thermal conductivity, although some results have appeared quite recently[60,61]. For the former, the appropriate expression to evaluate in a computer simulation study is given in Eq. (3.38), which we write here as

$$\eta_B = (\tfrac{1}{9} V k_B T) \sum_{\lambda,\mu} \int_0^\infty dt \langle \sigma'^{\lambda\lambda}(0) \sigma'^{\mu\mu}(t) \rangle \tag{4.13}$$

It was pointed out in Section 3 that the explicit form of $\sigma'^{\lambda\lambda}$ depends on the type of ensemble used. The results in Ref. 60 were obtained for a microcanonical ensemble, and in this case the stress tensor takes the form

$$\sigma'^{zz}(t) = \sum_j \{ m v_j^z(t) v_j^z(t) + r_j^z(t) F_j^z(t) \} - N k_B T - \tfrac{1}{3} \sum_j \langle \mathbf{r}_j \cdot \mathbf{F}_j \rangle \tag{4.14}$$

The last two terms refer to the kinetic and potential contributions to the $PV$ term respectively. The Green-Kubo result for the thermal conductivity, $\lambda$, is stated in Eqs (3.33) and (3.34). In both cases the integrand can be broken down into kinetic, potential and cross terms. An analysis of the correlation functions at liquid densities leads to the following conclusions: i) The overwhelming contribution to the transport coefficient comes from the purely potential part of the correlation function. ii) The correlation function for $\lambda$ shows a slower initial decline than its bulk viscosity counterpart, although it eventually decays much more rapidly. It also appears less sensitive to the system size and length of computer run.

The values obtained from Ref. 60 and 61 for $\eta_B$ and $\lambda$ are given in Table 4.1. They are in reasonable agreement with the available experimental data. Computer data for $\eta$ and $D$ are included for completeness.

Vogelsang and Hoheisel[62] have recently carried out a more systematic comparison of the simulation and liquid argon data. Agreement between them is excellent except for states of high temperatures and pressure.

### *4.3 Liquid Metal-Like Systems*

In spite of the large amount of experimental data for the shear viscosity of liquid metals very few comparisons exist with simulation results. Atomic transport in liquid

**Table 4.1** Bulk viscosity and thermal conductivity data from computer simulation of argon (Hoheisel, Vogelsang and Schoen[60]).

| $n \times 10^{-24}$ ($cm^{-3}$) | $T(K)$ | $\eta_B(mP)$ | $\lambda \times 10^5$ ($cal\ cm^{-1}\ s^{-1}\ K^{-1}$) | $\eta(mP)$ | $D \times 10^5$ ($cm^2\ s^{-1}$) |
|---|---|---|---|---|---|
| 0.01061 | 150 | 0.50 | 7.18 | 0.34 | 16 |
| 0.01519 | 219.6 | 0.49 | 16.51 | 0.73 | 14 |
| 0.01583 | 139.7 | 0.67 | 14.83 | 0.77 | 8.2 |
| 0.01824 | 120.3 | 0.81 | 20.81 | 1.09 | 4.8 |
| 0.01882 | 309.1 | 0.68 | 25.60 | 1.33 | 11.7 |
| 0.02029 | 116.5 | 0.73 | 28.47 | 1.97 | 3.7 |
| 0.02029 | 225.4 | 0.66 | 28.23 | 1.75 | 6.4 |
| 0.02138 | 85.5 | 1.05 | 28.47 | 2.97 | 1.72 |
| 0.02161 | 81.8 | 1.05 | 32.54 | 3.08 | 1.5 |
| 0.02593 | 221.3 | 1.02 | 59.57 | 6.09 | 2.3 |
| 0.02634 | 303.4 | 0.82 | 59.57 | 4.78 | 3.5 |

sodium and potassium has been studied by Berezhkovsky *et al.*[63], using an effective pair potential of the form[64]

$$\varphi(r) = (Ze)^2/r - [2(Ze)^2/\pi] \int_0^\infty dk F(k) \sin(kr)/kr \tag{4.15}$$

The second term accounts for the indirect interaction between ions via the electron gas. This expression is derived within the pseudopotential framework, and $F(k)$ is given by[65]

$$F(k) = -[V^2k^4/16\pi^2(Ze)^2][1/\varepsilon(k) - 1]|v_{ps}(k)|^2 \tag{4.16}$$

with $\varepsilon(k)$ the dielectric function of the electrons and $v_{ps}(k)$ the Fourier transform of the electron-ion pseudopotential (assumed to be local). The Ashcroft empty-core model[66] was used for the latter. In comparing the resulting pair potential with the LJ type, one notices that it tends to be softer at short range, has a deeper minimum and displays weak oscillations at long distances. The values of the shear viscosity, obtained by evaluating the Green-Kubo integrand, turn out to be $\approx 30\%$ lower than the corresponding experimental data in the whole range of temperatures investigated both for sodium and potassium. The details are given below, in Tables 4.2 and 4.3, along with results for the self-diffusion coefficient.

In the same paper the bulk viscosity is also reported, but more interesting is a result for the self diffusion coefficient. Unfortunately, comparison with experiment is possible only at the lowest temperature. Agreement turns out to be good for sodium but poor for potassium. Moreover, an empirical formula proposed by Tanaka[55] for rubidium, gives a good representation of the potassium data when it has the form

$$D = 4.38 \times 10^{-5}(T_m/M)^{1/2}V(T)^{1/3}(T/T_m)^{2.24}\ \mathrm{cm^2\ s^{-1}} \tag{4.17}$$

In this expression, $M$ is the atomic weight and $V(T)$ the atomic volume (in $Å^3$) of the saturated liquid at temperature $T$. A fit of the sodium diffusion data was not possible with a formula of this type, and an Arrhenius expression was not appropriate either.

**Table 4.2** Self-diffusion and shear viscosity coefficients of liquid sodium along the saturated vapour-pressure curve (Berezhkovsky *et al.*[63]).

| $T(K)$ | $D \times 10^5$ ($cm^2\,s^{-1}$) *MD* | $\eta(mP)$ *MD* | $\eta(mP)$ *Exp* |
|---|---|---|---|
| 393 | 0.50 (0.48*) | 4.50 | 6.20 |
| 573 | 1.2 | 2.35 | 3.35 |
| 800 | 2.2 | 1.71 | 2.30 |
| 1073 | 3.7 | 1.20 | 1.65 |
| 1500 | 7.2 | 1.26 | 1.24 |
| 1800 | 9.8 | 0.87 | 1.07 |

* Experiment

**Table 4.3** Self-diffusion and shear viscosity coefficients of liquid potassium along the saturated vapour-pressure curve (Berezhkovsky *et al.*[63]).

| $T(K)$ | $D \times 10^5$ ($cm^2\,s^{-1}$) *MD* | $\eta(mp)$ *ND* | $\eta(mp)$ *Exp* |
|---|---|---|---|
| 393 | 0.43 (0.65*) | 3.75 | 3.85 |
| 573 | 1.02 | 1.75 | 2.25 |
| 1073 | 3.70 | 0.80 | 1.15 |
| 1500 | 7.66 | 0.74 | 0.93 |
| 1800 | 9.99 | 0.61 | 0.79 |

* Experiment



The shear viscosity of liquid rubidium has been evaluated by Balucani *et al.*[67], at two temperatures and density close to the melting point, and at two other states along the coexistence curve. The values obtained are summarized in the table below, along with some experimental results[68].

The potential model used in the simulation is obtained from Eqs (4.15) and (4.16), using a dielectric function and empty-core radius given by Price *et al.*[69]. The good agreement with the experimental data gives some confidence in the ability of the pair potential, in this instance, to reproduce the dynamical behaviour of the real physical system. In Ref. 67 a detailed analysis of the stress autocorrelation function has been

**Table 4.4** Shear viscosity coefficients in liquid rubidium.

| $T(K)$ | $n^*$ | $\eta(mP)$ *MD* | $\eta(mP)$ *Exp* |
|---|---|---|---|
| 318 | 0.9045 | 6.10 | 5.95 |
| 338 | 0.9045 | 5.50 | 5.93 |
| 625 | 0.7965 | 2.30 | 2.34 |
| 942 | 0.7111 | 1.30 | 1.55 |

performed by comparing the MD result with a calculation based on the mode-coupling theory (see Fig. 6.1).

### *4.3 Non Equilibrium Methods*

The problems associated with the accurate evaluation of the long time tail of the correlation functions and the intrinsic limitations imposed by the finite size of the system, has stimulated a different approach to the calculation of transport coefficients which is normally referred to as Non-Equilibrium Molecular Dynamics (NEMD). In their pioneering work Ashurst and Hoover[70], evaluated the shear viscosity of soft spheres and LJ particles by molecular dynamic modelling of Couette flow. For fluid flow in, say, the $x$ direction the periodic boundary conditions in the $z$ direction are released and substituted by special boundaries which produce the desired non-equilibrium flux. That is, the $z$ faces of the containing walls are replaced by two lattice layers, each consisting of a small number of particles with the same spatial correlations as the bulk fluid but fixed positions; the shear flow is induced by translating the two layers in opposite directions. External forces are applied only within the fluid-wall regions to maintain the desired velocity gradient in the $z$-direction. The shear viscosity coefficient is then determined from the measured velocity gradient set up along the $x$ direction and the external shear force per unit area given by

$$P_{xz} = -\eta du_x/dz \tag{4.18}$$

In fact this relationship holds only when the shear stress is sufficiently small that higher order powers in the velocity gradients are negligible. An extrapolation to zero shear rate is then necessary to derive the correct value of the shear viscosity coefficient. The results obtained for the LJ fluid compared very favourably with those obtained by the standard MD method and the experimental data for argon. Calculations of the thermal conductivity of a LJ system by imposing a temperature gradient between two walls of the simulation cell, have been reported by Ciccotti *et al.*[71]

The major difficulty of this NEMD method arises from the possible onset of large inhomogeneities, induced by the small size of the systems investigated, which produce a degree of uncertainty in the interpretation of the results. This method is now largely confined to very specialized applications (see for example Ref. 72).

In the second NEMD method the system is not driven by artificially imposed boundary conditions, but, instead, the equations of motion are modified by the introduction of a fictitious external field, $F_{ext}$. If the transport coefficient, $L$, has been identified by its Green–Kubo relation

$$L = (1/k_B T) \int_0^\infty dt \langle J_1(0) J_1(t) \rangle \tag{4.19}$$

the external field $F_{ext}$, is *invented* such that its coupling with the system yields a dissipative flux $J_1(t)$. The steady state average $\langle J_1(t) \rangle_{NE}$ is computed, and on the basis of linear response theory we have the result

$$L = \lim_{F_{ext} \to 0} \lim_{t \to \infty} \langle J_1(t) \rangle / F_{ext} \tag{4.20}$$

Equation (4.20) holds only under the following conditions: (i) the new equations of motion are periodic, and (ii) the equations of motion generate trajectories in a phase space which fulfills the adiabatic incompressibility condition. The existence of a Hamiltonian, from which to derive the equations of motion, is a sufficient (but not necessary) requirement for condition (ii) to be satisfied.

Various algorithms have been proposed for the calculation of self-diffusion[73], shear viscosity[74,75,76] and thermal conductivity[77]. A detailed review of the NEMD technique has been given by Evans[78].

A very delicate point in the evaluation of transport coefficients through NEMD simulation is the proper extrapolation to zero external field strength, $F$, which is implicit in Eq. (4.20). For example in the case of the shear viscosity it has been argued[79] that

$$\eta(\gamma) = \eta(0) - \eta'\gamma^{1/2} \tag{4.21}$$

where $\gamma$ is the particular form of $F$ for shear viscosity, namely the imposed strain rate. This result has been tested by Cummings and Morriss[80] in a NEMD simulation for the shear viscosity of liquid Rb at the triple point. They conclude that although Eq. (4.21) is modified by terms proportional to $\gamma^2$, the leading effect is provided by $\gamma^{1/2}$. However, it should be noted that recent long simulation runs[81] have shown that at low values of $\gamma$, $\eta(\gamma)$ appears to be independent of the field strength. If so, this would imply that the evaluation of $\eta$ by means of Eq. (4.21) could lead to a substantial overestimate. The controversial nature of this aspect of the technique also arises in the calculation of the thermal conductivity. Recent work[82] has suggested that the *linear* behaviour with field strength, which has been assumed earlier[77], may break down at sufficiently small values of the field.

Finally, we mention recent extensive evaluation of transport coefficients in Lennard-Jones systems[83], using both Green-Kubo and NEMD simulation techniques. An important objective of this work was to use the results to test the reliability of a hard-sphere description of the data in terms of a temperature-dependent sphere diameter. A similar type of analysis is the subject of Section 5.



## 5 THE RIGID SPERE SYSTEM AND MODELS FOR ATOMIC TRANSPORT IN LIQUIDS

The rigid sphere model has been successfully used to interpret the static structure and thermodynamic properties of dense simple liquids[84]. There is extensive information about transport coefficients in a rigid sphere fluid from both theory and computer simulation studies, and it is an inviting prospect to make this information the basis of a discussion of transport properties of simple liquids. By doing this we are assuming that the mechanisms for the transfer of particles, momentum and energy in the liquid are essentially the same as for rigid spheres. In the case of diffusion, for example, computer studies of rigid sphere systems support the contention that it is not realistic to extend to liquids the type of theory used to explain diffusion in solids, involving potential barriers and an activation energy necessary for an atom to move into an

available vacancy. Instead, the physical picture of the mechanism as a gas-like process emerges, but with mean free paths which are a fraction of an atomic diameter, so that diffusion occurs predominantly by a succession of small displacements[85].

### 5.1 *The rigid Sphere Fluid*

In Section 3 an exact expression for each transport coefficient was obtained in terms of a Green-Kubo relation. Before we take the rigid sphere fluid seriously as a model for transport in simple liquids we should investigate some of the details of the appropriate time-dependent autocorrelation functions. The instantaneous nature of the rigid sphere interaction, in fact, results in a different type of structure for the correlation functions, particularly at small times, when compared to results for liquids with continuous, differentiable potentials. The pertinent question to ask is how this affects the calculated values of transport coefficients.

Once again, consider single particle motion and self-diffusion as an illustrative example. The appropriate normalized correlation function in the Green-Kubo relation (3.11) is the velocity autocorrelation function, $\psi(t) \equiv (3k_B T/m)^{-1}\langle \mathbf{v}_1(0)\cdot\mathbf{v}_1(t)\rangle$, and it is useful in the discussion to introduce the associated memory function $K(t)$. As shown, for example, in Boon and Yip[86] we may write

$$K(t) = \zeta(t) - \int_0^t ds K(t-s)\dot{\psi}(s) \tag{5.1}$$

where $\zeta(t) = \langle \mathbf{F}_1(0)\cdot\mathbf{F}_1(t)\rangle/(3mk_B T)$ and $\langle \mathbf{F}_1(0)\cdot F_1(t)\rangle$ is the force autocorrelation function. It follows that $K(t) \approx \zeta(t)$ can be useful in discussing the short-time dynamics of the memory function, since the latter's time evolution is governed by the anomalous propagator which makes it less transparent.

It is readily demonstrated, for example, that

$$\zeta(0) = K(0) = (\tfrac{1}{3}mk_B T)\Big[\Big\langle \sum_{i\neq 1} (\nabla\varphi(r_{1i}))^2\Big\rangle + \Big\langle \sum_{i\neq 1}\nabla\varphi(r_{1i})\cdot\sum_{j\neq 1,i}\nabla\varphi(r_{1j})\Big\rangle\Big] \tag{5.2}$$

Note that the evaluation of the first term in Eq. (5.2) involves the two- and the second the three-particle distribution function. As shown by Schofield[87], we may also write this equation as

$$K(0) = -(4\pi n/3m)\int_0^\infty drr^2 y(r)f'(r)\varphi'(r) + (4\pi n/3m)\int_0^\infty drr^2 y'(r)f'(r) \tag{5.3}$$

where the expressions on the right hand side are respectively the equivalents of those in Eq. (5.2), and we have introduced $f(r) = \exp(-\varphi(r)/k_B T) - 1$ and $y(r) = g(r)\exp(\varphi(r)/k_B T)$. We now consider the situation when the steepness of a repulsive potential increases to the hard sphere limit. Take $\varphi(r)$ to be the inverse power potential $\varepsilon(\sigma/r)^\nu$. Bearing in mind that $f(r) \to \delta(r-\sigma)$ as $\nu \to \infty$, we have

$$K(0) \approx (4\pi n\sigma/3m)[y(\sigma)\varepsilon\nu + \sigma y'(\sigma)]$$

showing that the pair contribution to $K(0)$ diverges as $v$, while the triplet contribution remains finite. Introducing a length $\Delta$, through the equation $(\sigma/\sigma - \Delta)^v = e$, as a measure of the penetration depth during a collision, we obtain $\Delta \approx \sigma/v$ for large $v$. An effective estimate of a binary collision time, and hence the relaxation time of the binary contribution to $\zeta(t)$, is given by $\Delta/v_0 = (\sigma^2 m/k_B T)^{1/2} v^{-1}$ when $v_0 = (k_B T/m)^{1/2}$ is the thermal speed of a particle.

Thus, as the rigid sphere limit is approached, the initial value of $K(t)$ diverges as $v$ while its decay time (like that of $\zeta(t)$) tends to zero like $v^{-1}$. It follows that the integral of the binary collision component, and hence its contribution to the transport coefficient, remains finite *and relatively insensitive to the hardness of the repulsive core of the potential.* The latter is an important conclusion in a consideration of the relevance of the rigid sphere model[87]. In view of the above discussion, we expect that for rigid spheres the memory function has the structure

$$K(t) = 2\Omega\delta(t) + k(t) \tag{5.4}$$

The delta function describes the effect of binary encounters and $k(t)$, which remains finite as $t \to 0$, the influence of correlated sequences of collisions. As defined above, $\Omega$ is the time derivative of $\psi(t)$ at $t = 0$, and is given exactly by

$$\Omega = (8n\sigma^2 g(\sigma)/3)(\pi k_B T/m)^{1/2} \tag{5.5}$$

where $g(\sigma)$ is the contact value of the radial distribution function.

For the other transport coefficients the purely potential terms in the Green-Kubo integrands make the dominant contributions at liquid densities. In each case, the binary collision effects arise from the strictly two-body force correlation whose initial values again diverge with the steepness of the potential. In the rigid sphere limit they produce a delta function behaviour in the Green-Kubo integrand itself. Using the result from Eq. (3.11) that the self-diffusion coefficient is obtained as

$$D = (k_B T/m)\int_0^\infty dt\psi(t) = (k_B T/m)\left[\int_0^\infty dt K(t)\right]^{-1} \tag{5.6}$$

and including only the binary collision contribution to the memory function, it follows that $D = k_B T/m\Omega$. From the similarity of the two-body correlations involved in each case, it can be shown that the binary collision contributions to the transport coefficients (denoted by label b) are related through the equations

$$\Omega = k_B T/mD^b = 10\eta^b/nm\sigma^2 = 6\eta_B^b/nm\sigma^2 = 4\lambda^b/nk_B\sigma^2 \tag{5.7}$$

It is interesting to compare these results with Enskog theory[88]. The result for $D^b$, in fact, coincides with the Enskog approximation for the diffusion coefficient, namely

$$D_E = (3/8n\sigma^2)(k_B T/m\pi)^{1/2} g(\sigma)^{-1} \tag{5.8}$$

Enskog results for the shear viscosity and thermal conductivity coefficients include kinetic and cross terms as well as the purely potential contributions. They are frequently given in the form

$$\begin{aligned}\eta_E &= \eta_0[g(\sigma)^{-1} + 0.8x + (48/25\pi)g(\sigma)x^2 + 0.150g(\sigma)x^2] \\ \lambda_E &= \lambda_0[g(\sigma)^{-1} + 1.2x + (32/25\pi)g(\sigma)x^2 + 0.340g(\sigma)x^2]\end{aligned} \tag{5.9}$$

**Table 5.1** Ratios of computed hard-sphere transport coefficients to the Enskog values (Alder, Gass and Wainwright[50]).

| $V/V_0$ | $D/D_E(e)$ | $\eta/\eta_E$ | $D\eta\sigma/k_BT$ | $\lambda/\lambda_E$ | $\eta_B/\eta_B^E$ |
|---|---|---|---|---|---|
| 100 | 1.02 | 1.01 ± 0.02 | | 0.98 ± 0.02 | 0.9 ± 0.2 |
| 20 | 1.04 | 1.00 ± 0.02 | | 0.99 ± 0.02 | 1.1 ± 0.2 |
| 10 | — | 0.99 ± 0.04 | | — | — |
| 5 | 1.16 | 0.99 ± 0.05 | 0.156 | 0.97 ± 0.03 | 0.9 ± 0.2 |
| 3 | 1.34 | 1.02 ± 0.01 | 0.147 | 1.00 ± 0.01 | 0.98 ± 0.07 |
| 2 | 1.27 | 1.11 ± 0.06 | 0.157 | 1.02 ± 0.03 | 0.9 ± 0.2 |
| 1.8 | 1.15 | 1.10 ± 0.03 | 0.147 | 1.03 ± 0.02 | 1.1 ± 0.2 |
| 1.6 | 0.84 | 1.44 ± 0.07 | 0.150 | 1.05 ± 0.02 | 1.1 ± 0.2 |
| 1.5 | 0.58 | 2.16 ± 0.09(a) | 0.168 | 1.05 ± 0.03(a) | 0.6 ± 0.2 |

(*e*) Extrapolated to infinite system.

(*a*) 500 particle system. All other data refer to 108 particle system.

where $x = (2\pi n\sigma^3/3)$, and $\eta_0 = (5/16\sigma^2)(mk_BT/\pi)^{1/2}$ and $\lambda_0 = k_B(75/64\sigma^2) \times (k_BT/\pi m)^{1/2}$ are dilute gas values of the coefficients. The first and second terms on the right hand side, in both the above equations, correspond to kinetic and cross terms respectively. The third gives the exact binary collision component and the last an estimate of further collision effects. There are slightly different estimates of the latter quoted in the literature. In the shear viscosity coefficient, Resibois[89], for example, has a value of $(4/25)\eta_0 g(\sigma)x^2$, rather than $0.150\eta_0 g(\sigma)x^2$; and for the thermal conductivity, $(9/25)\lambda_0 g(\sigma)x^2$ instead of $0.340\lambda_0 g(\sigma)x^2$. Only collisional effects contribute to the rigid sphere bulk viscosity, and the Enskog value is dominated by the binary collisions, so that

$$\eta_B^E = \eta_B^b = \eta_0[(16/5\pi)g(\sigma)x^2] \tag{5.10}$$

However, Resibois again includes a minor addition to this expression, in his version of the Enskog approximation, which increases the numerical factor by 8/225.

In Table 5.1 the Enskog theory predictions are compard with the molecular dynamics results of Alder, Gass and Wainwright[50]. The extrapolated values for infinite systems are obtained from the latter reference, but note that later work suggests that the procedure may have overestimated the corrections[90]. Nevertheless, the deviations from $D_E$ and $\eta_E$ are particularly marked as the density increases and $V/V_0(=\sqrt{2}/n\sigma^3)$ becomes $\leq 2.0$, $V_0$ being the volume occupied by the spheres at close packing.

The Stokes–Einstein relationship between $D_{HS}$ and $\eta_{HS}$, for slip boundary conditions, takes the form $D = k_BT/4\pi\eta(\sigma/2)$. Although this is derived for a 'large' spherical particle immersed in a continuous medium, a noteworthy feature of the above results is that it appears to be applicable to the rigid sphere fluid. The fourth column in the above table shows that the quantity $D\eta\sigma/k_BT$ is strikingly constant for $V/V_0 \leq 5$, and very close to the value $1/2\pi(=0.159)$. A more detailed discussion of the Stokes–Einstein relationship, valid also for dense systems with continuous potentials, will be presented in Section 6.

Microscopic theories of all aspects of the dynamics of a rigid sphere fluid, which attempt to improve Enskog theory (with varying degrees of success), are not in short

supply. The later studies have involved developments of kinetic theory in conjunction with a form of mode-coupling approximation (see Section 6 for a discussion of the physical concepts behind this approach). Despite their interest and importance, such theories are not our principal concern here, and we refer the reader to the work of Leutheusser[91] as a recent example, and for a list of references. The work of Resibois[89], Furtado *et al.*[92] and Sung and Stell[93] is also mentioned because specific calculations of the velocity autocorrelation function and/or self-diffusion coefficient were made, over a wide range of packing fractions, to try to explain the density dependence of the simulation data for $D$. In spite of these efforts, when using the rigid sphere fluid as a basis for the interpretation of transport properties of liquids, the most useful procedure remains some form of phenomenological approach. This makes use of fitted forms for the ratios shown in Table 5.1, which have some simple dependence on $V/V_0$.

### 5.2 *Models of Atomic Transport Coefficients in Liquids*

Dymond[94] has proposed some practical methods of achieving such a rigid sphere model of atomic transport in simple liquids. For diffusion, he found it useful to define a dimensionless quantity

$$D^* = g(\sigma)^{-1}(V/V_0)(D_{HS}/D_E) \tag{5.11}$$

which could be calculated from the computer results and fitted to a linear function of $V/V_0$, namely,

$$D^* = 1.271[V/V_0 - 1.384] \tag{5.12}$$

Over the range $1.5 \leq V/V_0 \leq 2.0$ the accuracy is within 2%. Using the result for $D_E$ and the equation $N\sigma^3 = \sqrt{2}V_0$, from which $\sigma^2 = (\sqrt{2}V_0/N)^{2/3}$, we obtain

$$D^* = D_{HS}(8/3)(\pi M/RT)^{1/3}(2N/V_0)^{1/3} \tag{5.13}$$

$M$ is the molar mass and $R$ the gas constant. Combining the last two equations, and using molar values of $N$ and $V$ it follows that

$$\begin{aligned} D_{HS} &= 2.257(RT/M)^{1/2}V_0^{-2/3}[V - 1.384V_0]10^{-5} \\ &= 2.306(T/M)^{1/2}V_0^{-2/3}[V - 1.384V_0]10^{-5}\ \text{cm}^2\ \text{s}^{-1} \end{aligned} \tag{5.14}$$

In relation to the viscosity and thermal conductivity he also pointed that within the uncertainty of the computer data, and for $1.5 \leq V/V_0 \leq 3$, $\eta_0/\eta_{HS}$ can be reproduced by the expression

$$\eta_0/\eta_{HS} = 0.2195[V/V_0 - 1.384]$$

and for $1.5 \leq V/V_0 \leq 2$, $\lambda_0/\lambda_{HS}$ by

$$\lambda_0/\lambda_{HS} = 0.1611[V/V_0 - 1.217]$$

In terms of practical units these equations become

$$\eta_{HS}^{-1} = 14520(MT)^{-1/2}V_0^{-1/3}[V - 1.384V_0] \tag{5.15}$$

with $\eta_{HS}$ in poise, and

$$\lambda_{HS}^{-1} = 1430(MT)^{1/2}V_0^{-1/3}[V - 1.27V_0] \tag{5.16}$$

where $\lambda_{HS}$ is in cal·cm$^{-1}$ s$^{-1}$ K$^{-1}$.

Within the rigid sphere model the above expressions for $D_{HS}$, $\lambda_{HS}$ and $\eta_{HS}$ are identified with the experimental transport coefficients of a liquid. Note that the form of these fits implies that $D\eta/T$ is constant, which is consistent with the Stokes-Einstein relationship between $D$ and $\eta$. When testing the applicability of these results to liquids it has to be appreciated that $V_0$ depends on the effective hard core diameter, $\sigma$. The latter is expected to depend on both temperature and density (or pressure). We discuss, below, a theoretical expression for the temperature dependence, but first consider a more empirical approach, used by Dymond[94]. He applied it to the interpretation of the transport properties of liquid carbon tetrachloride, whose molecules are roughly spherical, and for which accurate experimental data is available. Values for $V_0$ were obtained, along a number of isotherms, by fitting Eq. (5.15) at each data point of the measured viscosity[95] over a pressure range of 1500 atm. These were then used in Eq. (5.14) to calculate the self-diffusion coefficient on each isotherm. Very good agreement with experimental data[96] was obtained. A similar test using methane measurements along the saturated vapour pressure line also proved satisfactory. For methane, the effective core diameter determined from $V_0$, changed from 3.77 Å at 90.92 K to 3.63 Å at 153.5 K. Liquid metals data was investigated in the same way by van Loef[34]. Since, as we have stressed, data of the shear viscosity coefficient are generally more accurate and extensive than for $D$, he also used Eq. (5.15) to determine $V_0$ and hence $\sigma$. At constant pressure, and over a temperature range from the melting point ($T_M$) to $4T_M$, $\sigma(T)$ for the alkali metals decreased by about 15%. This is a greater reduction than van Loef reports for the effective core diameter in argon over a similar temperature range. This difference is qualitatively consistent with current theories of the effective pair potentials in liquid metals. As pointed out in Section 4, when compared with a typical Lennard-Jones 6-12 potential the repulsive part is somewhat softer, particularly for the alkali metals. Having obtained the effective diameter, Eqs (5.14) amd (5.16) can be used to predict $D$ and $\lambda$. The calculated values for $D$ and $\lambda$ show discrepancies of the order of $\pm 20\%$ when compared to experimental data for argon along the saturated vapour pressure curve. For the alkali metals there is a similar discrepancy for $D$ at the melting point ($\lambda$ of course is dominated by the electron contribution) but the values are systematically lower. The discrepancy decreases with increasing temperature. Despite its limitations, this type of approach can be made the basis of a useful practical means of correlating transport data over a wide range of experimental conditions.[97]

Another type of application of the rigid sphere model, proposed by Protopapas *et al.*[98], is to assign the core diameter the average distance of closest approach in a binary collision. At contact, therefore, the pair potential should be proportional to $k_BT$ i.e. $\varphi(r = \sigma(T)) = \alpha k_BT$. It is assumed, also, that between the potential minimum, $\sigma_m$, and $\sigma(T)$ the potential has a parabolic shape i.e. $\varphi(r) = A(r - \sigma_m)^2$, where $A$ like $\alpha$ is a proportionality constant. From these two conditions it follows that

$$\sigma(T) = \sigma_m - (\alpha k_BT/A)^{1/2} \tag{5.17}$$

and from its application at the melting point it is readily shown that

$$\sigma(T) = \sigma_m[1 - B(T/T_M)^{1/2}] \tag{5.18}$$

with $B = (\sigma_m - \sigma(T_M))/\sigma_m = (\sigma k_B T_M/A\sigma_m^2)^{1/2}$. The packing fraction at the melting temperature, $\mu_M$, is introduced so that $\mu_M = (\pi n_M \sigma(T_M)^3)/6$, with $n_M$ the number density of the liquid. Combining this with Eq. (5.18) gives

$$\sigma(T) = (6\mu_M/\pi n_M)^{1/3}[1 - B(T/T_M)^{1/2}]/(1 - B) \tag{5.19}$$

This result for $\sigma(T)$ is used in an expression for $D$ given by

$$D = g(\sigma)^{-1}(3/8n\sigma^2)(k_B T/\pi m)^{1/2}(D_{HS}/D_E) \tag{5.20}$$

which, in the spirit of Dymond's approach, is identified with the self-diffusion coefficient of the liquid. The ratio $D_{HS}/D_E$, which depends only on the packing fraction of the fluid, is obtained from Alder and Wainwright's data. The contact value of the radial distribution function, $g(\sigma)$, is also determined by the packing fraction and the sphere diameter. Thus, given the number density of the liquid, the packing fraction is calculated in terms of $\sigma(T)$, and only two parameters $\mu_M$ and $B$ are required to predict the transport coefficient. These are determined in an empirical fashion. The packing fraction is estimated by fitting $D$ to the experimental value at the melting point. For the liquid metals investigated a value of about 0.472 was obtained, and adopted for all liquid metals. Table 5.2 shows the accuracy of the fit which was achieved with $\mu_M = 0.472$. The parameter $B$ is determined by selecting it to fit the experimentally determined temperature dependence of the diffusivity. Protopapas[99] found, rather surprisingly, that the same value of $B = 0.112$ could describe all metals for which data is available (bearing in mind the scatter in the data, and the differences between the results of different experiments). Some attempt to understand this result has been made[98].

**Table 5.2** Comparison of melting point values for $D \times 10^5$ ($cm^2\,s^{-1}$). The experimental values are from a number of sources (Protopapas, Anderson and Parlee[98]), the calculations are based on Eqs (5.20) and (5.19).

| *Element* | *Experiment* | *Calculated* |
|---|---|---|
| Li | 6.80 | 7.01 |
| Na | 4.22 | 4.24 |
| K | 3.82 | 3.85 |
| Rb | 2.62 | 2.68 |
| Cu | 3.96 | 3.40 |
| Ag | 2.55 | 2.77 |
| Zn | 2.05 | 2.55 |
| Cd | 1.78 | 2.00 |
| Hg | 1.17 | 1.07 |
| Ga | 1.72 | 1.73 |
| In | 1.74 | 1.77 |
| Sn | 2.05 | 1.96 |
| Pb | 1.68 | 1.67 |
| Ar | 1.53 | 1.57 |

The predicted variation of the self-diffusion coefficient with temperature is also demonstrated in the latter reference. For some liquid metals the theory predicts the temperature dependence of experimental diffusion data fairly successfully—although the temperature range involved is usually of the order of 200–300 degrees only. For others, it is less convincing. The predictions of an alternative hard sphere model[100], and those of quite different theories are also summarized in Ref. 98.

In all these approaches some implicit assumptions are made about the transport mechanism. A number of them, for example, predict reasonable values for the self-diffusion coefficient despite the fact that different concepts of the underlying mechanism are involved. Another point of concern is that they fail to correlate the assumed transport process with the time dependence of the Green-Kubo integrands (i.e. the atomic dynamics), as determined by computer simulation. In Section 6 we avoid preconceived ideas and discuss attempts to predict transport coefficients from microscopic theories of the relevant autocorrelation functions.

## 6 MORE ADVANCED THEORETICAL METHODS: INTERRELATIONSHIPS BETWEEN TRANSPORT COEFFICIENTS.



As we saw in Section 3, ordinary transport coefficients enter into the dynamics of quasi-conserved variables and directly control the (slow) decay of the corresponding time correlation functions for small wavevectors. In turn, transport coefficients are expressible in terms of Green-Kubo integrals involving generalized "fluxes". From Eq. (3.6), the time evolution of the latter is seen to proceed in a subspace orthogonal to the one spanned by the "slow" variables. It may seem appropriate therefore, to assume that the decay of the Green-Kubo integrands can be considered fast enough to be described by simple approximation schemes which involve only limited information of the short time dynamics. An example of such a procedure has indeed been given in Section 5, where the result $D \approx k_B T/m\Omega$ was obtained, $\Omega$ being the initial slope of the Green-Kubo integrand, in this case the velocity autocorrelation function.

Although reasonable, we small see that the argument has some internal inconsistency which makes its applicability more and more doubtful as the density of the system increases and/or the temperature decreases. The Green-Kubo integrands may, for example, develop relatively long-lasting effects which are neglected in the simple approximation schemes and which may give significant contributions to the values of the transport coefficients. This is demonstrated in Table 5.1. for the rigid sphere fluid, where the discrepancies between the computed values of $D$ and $\eta$ and their Enskog values (predominantly determined by uncorrelated binary collisions) become quite evident at large and even intermediate densities. In the last decade a rather comprehensive theoretical framework has emerged to try to calculate and explain these effects in the dynamics of simple liquids. It combines the concepts of kinetic theory (usually employed at low densities) with suitable projection operator techniques, referred to as mode-coupling theory. As anticipated in Section 5, we shall not attempt a detailed account of these methods (cf. Refs 101, 102 for a review); however,

since mode-coupling techniques are particularly suited to a description of dynamical effects at intermediate and long times, a brief discussion of the latter is appropriate here.

The main internal inconsistency alluded to in the last paragraph is that the orthogonality of the random forces to the "slow" variables $\hat{A}_i(\mathbf{k} \to 0)$ does not necessarily mean that the memory function has only rapidly varying components. It is possible to form products of the variables ("modes") i.e. $(1 - P)\hat{A}_i(\mathbf{q})\hat{A}_j(|k - \mathbf{q}|)$, $(1 - P)\hat{A}_i(\mathbf{q})\hat{A}_j(\mathbf{q}')\hat{A}_k(|\mathbf{k} - \mathbf{q} - \mathbf{q}'|)$ etc., which are also slowly varying for sufficiently small $q$, $q'$, etc. Due to the presence of $(1 - P)$, these products lie in the same subspace as the random forces which may have a non-zero projection on them. Consequently, one can see that the random forces, and hence the memory functions and corresponding Green-Kubo integrands, may have features which vary only relatively slowly with time. In practice, almost all applications of mode-coupling theory have considered only bilinear products of $A_i$ variables, although even then there are an infinite number of such products, corresponding to all allowed $\mathbf{q}$'s in the system.

### 6.1 *Mode-Coupling Theory*

The technique is illustrated with two examples:

i) The first is provided by the derivation of an expression for the velocity autocorrelation function. As discussed in Section 3.2(a), this Green-Kubo integrand for the diffusion coefficient is derived from the memory function $K_s(k, t)/k^2$ (associated with the self-correlation function $F_s(k, t)$) in the $k \to 0$ limit. The first relevant variable to consider in the bilinear point is the single particle density $\hat{n}_s(\mathbf{q}, t)$; the second has necessarily to be a current in order to have a non-zero projection on the random force, which is proportional to the particle velocity. Thus, the product reads $B(\mathbf{k} \to 0) = \hat{n}_s(\mathbf{q})\hat{P}^\alpha(-\mathbf{q})$, where $\alpha$ runs over the cartesian components of the momentum density defined in Eq. (3.1). The projection operator $P \equiv P_s$ has been omitted, since in this case it gives zero contribution. Within mode-coupling theory the random force is given by its projected component onto the variables $B(\mathbf{k} \to 0)$ i.e.

$$
\begin{aligned}
&f(\mathbf{k} \to 0, t) \\
&\quad = \sum_{\mathbf{q}} \sum_{\alpha} \langle i\mathbf{k} \cdot \mathbf{v}_1 \hat{n}_s(\mathbf{q})\hat{P}^\alpha(-\mathbf{q})\rangle [\langle \hat{n}_s(q)\hat{P}^\alpha(-\mathbf{q})n_s^*(\mathbf{q})\hat{P}^{\alpha *}(-\mathbf{q})\rangle]^{-1} \hat{n}_s(\mathbf{q}, t)\hat{P}^\alpha(-\mathbf{q}, t) \\
&\quad = ik(Nm)^{-1} \sum_{\mathbf{q}} \hat{n}_s(\mathbf{q}, t)P^z(-\mathbf{q}, t) \qquad (6.1)
\end{aligned}
$$

The projection coefficient ("vertex" function) is $(Nm)^{-1}$ and we have chosen $\mathbf{k}$ in the $z$ direction. It then follows that the velocity autocorrelation function is given by $\langle f(\mathbf{k} \to 0, 0)f^*(\mathbf{k} \to 0, t\rangle/k^2$. Within the ensemble average, the single particle densities and current components are factorized, a typical procedure in mode-coupling theory, so that we obtain[103]

$$
\begin{aligned}
\langle \mathbf{v}_1(0) \cdot \mathbf{v}_1(t)\rangle &\approx 3(Nm)^{-2} \sum_{\mathbf{q}} \langle P^z(-\mathbf{q}, 0)P^z(\mathbf{q}, t)\rangle \langle \hat{n}_s(\mathbf{q}, 0)\hat{n}_s(-\mathbf{q}, t)\rangle \\
&= [Nm^2(2\pi)^3]^{-1} \int_{q < q_c} d\mathbf{q} n^{-1} [C_L(q, t) + C_T(q, t)]F_s(q, t) \qquad (6.2)
\end{aligned}
$$

where the momentum density fluctuation correlation function has been expressed through its longitudinal and transverse components with respect to the direction of **q**. The integral cut-off emphasizes that the theory can be justified only when the integral is dominated by a limited range of wavevectors.

This result may be expected to apply at intermediate and long times, which in practice will be that regime where the wavevectors greater than $q_c$ are irrelevant, and the results become independent of the upper limit which may be taken to be $\infty$. At sufficiently long times, where the small $q$ components in the integral dominate, the currents may be given their hydrodynamic form. It is easily shown that the longitudinal part contributes terms which have an exponential decay, and that with $C_T(q,t) = Nmk_BT\exp[-(\eta/nm)q^2t]$ and $F_s(q,t) = \exp[-q^2Dt]$ we obtain

$$\langle \mathbf{v}_1(0)\cdot\mathbf{v}_1(t)\rangle_{mc} \approx (k_BT/4nm)[\pi(\eta/nm + D)t]^{-3/2} \tag{6.3}$$

In this way the theory predicts the celebrated $t^{-3/2}$ tail, in line with the result deduced from computer simulation data of the velocity autocorrelation function[51,104]. The experimental verification of this effect in liquid Na has recently been reported[105]. Through its formulation, mode-coupling theory emphasises the long time behaviour. It is not surprising, therefore, that Eq. (6.2) predicts unphysical results at very short times (in particular, a divergent value at $t = 0$ as $q_c \to \infty$).

ii) The second application concerns the memory function $K_T(k,t)$ (Eq. (3.13)) associated with the transverse current. In this context it is considered appropriate to project the random force onto the subspace of bilinear products of collective conserved variables. The set chosen consists of the three momentum current components plus the density fluctuation. We take advantage of the expectation that, at liquid densities and sufficiently small $k$, the potential contribution to the random force is the dominant one and neglect the rest. This assumption is completely confirmed by molecular dynamics data of the stress autocorrelation function[106]. It then follows that the vertex functions are zero for all decay channels of bilinear products of density and current density component fluctuations, other than those of two density modes. This is immediately obvious for a product of a density and current component, bearing in mind our simplification of the random force. Using the properties of the canonical ensemble it can also be demonstrated for the product of two current components. The surviving contribution leads to the result[107]

$$K_T(k,t) = (k_BT/16\pi^3nm)\int_{q,|\mathbf{q}-\mathbf{k}|<q_c} d\mathbf{q}[q^x]^2[(S|\mathbf{q}-\mathbf{k}|) - S(q))/S(|\mathbf{q}-\mathbf{k}|)S(q)]^2 \times F(|\mathbf{q}-\mathbf{k}|,t)F(q,t) \tag{6.4}$$

and from this, the relevant Green–Kubo integrand becomes

$$\eta_{pp}(t) = (k_BT/60\pi^2)\int_0^{q_c} dqq^4[s'(q)/S^2(q)]^2F^2(q,t) \tag{6.5}$$

This equation has been used recently to interpret molecular dynamics data of the stress autocorrelation function in a liquid Rb model[106]. A viscoelastic scheme leads to

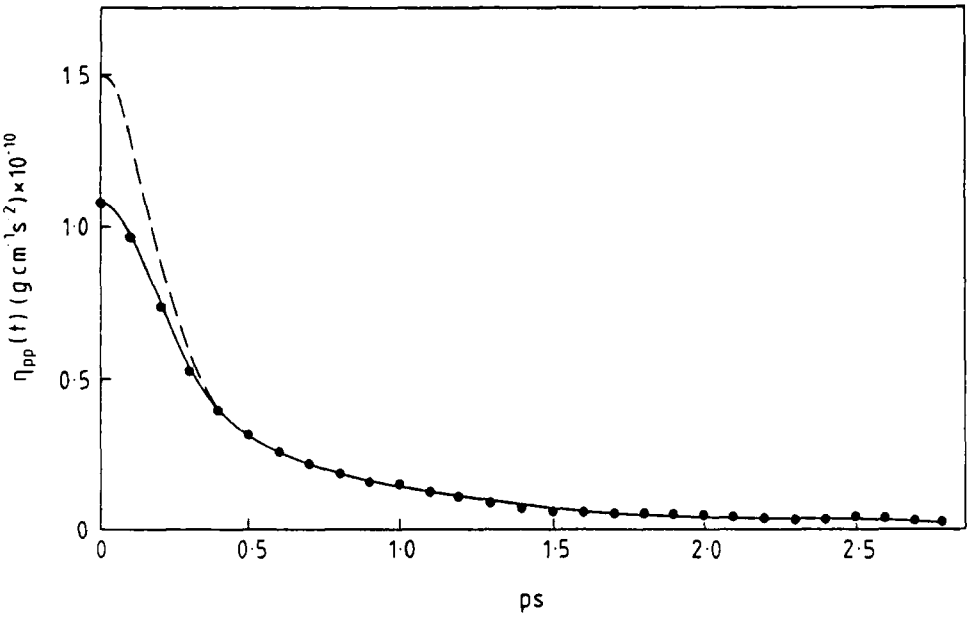


**Figure 6.1** Potential contribution to the stress autocorrelation function of liquid rubidium at $T = 338$ K. Dots: MD data. Full line: the mode-coupling result (Eq. (6.5)) with $q_c\sigma = 11.1$. Dashed line: the mode-coupling result with $q_c\sigma = 47.9$.



a realistic expression for the intermediate scattering function, $F(q, t)$, and $S(q)$ is taken from computer simulation results. The theoretical prediction of the time-dependence of $\eta_{pp}(t)$ is compared with simulation data in Figure 6.1, for two quite different values of $q_c$. For $t \geq 0.5$ ps, the choice of cut-off has no significant effect on the result, and this gives us confidence in the mode-coupling procedure for this time domain. Once again, the expression cannot be expected to reproduce the correct initial behaviour (although an extrapolation procedure has been devised to produce an excellent overall result and an accurate prediction of the viscosity[106]). For small $t$, a quite different treatment of the (rapid) dynamic events is clearly necessary. In addition to possible ansätze to model the initial decay of this and other correlation functions, some features of the short time dynamics may be incorporated by delaying the mode-coupling analysis to a later stage in the Mori continued fraction representation[108]. More satisfactory, are kinetic theory methods, combined with mode coupling techniques which have been successful in predicting the characteristic dynamical features at all times[109]. A consequence of this type of approach, which is indicated by the expressions in Eqs (6.2), (6.4) and (6.5), is that one correlation function tends to be expressed in terms of others. As a result, to be completely consistent within this framework, some correlation functions of interest, for example $F(k, t)$, have to be obtained by simultaneously solving several non-linear equations. The determination

of transport coefficients can become rather involved, and the physical processes of the transport mechanism obscured.

### 6.2 *Interrelationships Between Coefficients*

Writing one correlation function in terms of others can sometimes considerably simplify the problem of looking for interrelationships between transport coefficients. Examples have already been reported in Eq. (5.7), without the aid of mode-coupling theory. In that case, the simplicity of the results is a consequence of the binary collision approximation. Despite this, some of the predictions for the ratios of coefficients appear to be realistic for liquids, others are not. For example, from Eqs (5.7) we obtain $\eta/\lambda = 2m/5k_B$, which is in good agreement with the ratio of the experimental values for argon at the melting point. On the other hand, these equations give $\eta/\eta_B = 3/5$. For argon the ratio is $\approx 1.25$. It is safer to assume that at liquid densities different approaches have to be developed. In the following we shall discuss a microscopic derivation of the frequently used Stokes–Einstein relation between $D$ and $\eta$. Moreover, in this particular case it appears possible to establish for the Green–Kubo integrand involved a simple but consistent framework in which both the short- and long-time features are accounted for.



The starting point is again the velocity autocorrelation function. As is well known, in macroscopic treatments of a fluid a velocity field can be introduced, and implicitly defined by some coarse-grained average comprising a microscopically large number of particles. The concept can usefully be generalized at the microscopic level by introducing a velocity field of the form $\mathbf{v}(\mathbf{r}, t) = \sum_i \mathbf{v}_i(t) f(|\mathbf{r} - \mathbf{r}_i(t)|)$. The form factor $f(r)$ is constructed so that (i) the velocity field is essentially constant across an atomic diameter and (ii) the macroscopic sum rule $n \int d\mathbf{r} \mathbf{v}(\mathbf{r}, t) = \sum_i \mathbf{v}_i(t)$ is satisfied. For all practical purposes, both requirements can be met by choosing a step function form for $f(r)$, whose width, $a$, is determined by the condition $(4/3)\pi a^3 = 1$. By using the velocity field to evaluate the velocity autocorrelation function, one may exploit the relatively slow variation of atomic positions in the liquid with respect to the rate of momentum transfer, to arrive at[110]

$$\langle \mathbf{v}_1(0) \cdot \mathbf{v}_1(t) \rangle = [1/Nm^2(2\pi)^3] \int d\mathbf{q} \tilde{f}(q)[C_L(q, t) + 2C_T(q, t)]F_s(q, t) \qquad (6.6)$$

In this expression, $\tilde{f}(q) = (4\pi a^2/q) j_1(qa)$, is the Fourier transform of the $f(r)$ and $j_1(x)$ being a spherical Bessel function. Comparison with the mode-coupling result in Eq. (6.2) shows that the factor $1/n$ has been replaced by $\tilde{f}(q)$. Since $\tilde{f}(q \to 0) = 1/n$, Eq. (6.6) will predict the correct $t^{-3/2}$ decay of the correlation function. However, in contrast with Eq. (6.2), the physical requirements on $\mathbf{v}(\mathbf{r}, t)$ make Eq. (6.6) correct even at short times. It is easy to show that the latter equation reproduces both the initial value and short time decay of $\langle \mathbf{v}_1(0) \cdot \mathbf{v}_1(t) \rangle$. Moreover, with realistic models for $C_L$, $C_T$ and $F_s$, this result is found to account remarkably well for computer data of the velocity autocorrelation function even at intermediate times—including the so-called "cage effect"—for several systems in the liquid range[111].

A simplification of the above equation, by putting $F_s(q, t) = 1$, is made possible by the relatively slow variation of the atomic coordinates. This has a very minor effect on the results, a statement which is readily appreciated at long times, bearing in mind that in liquids $\eta/nm \gg D$. Integrating this simplified version of Eq. (6.6) with respect to time, and noting that there is no contribution from $C_L(q, t) = -(m/q^2)\ddot{F}(q, t)$, we obtain[112]

$$D = (1/3\pi^2 Nm) \int_0^\infty dq q^2 \tilde{f}(q) \int_0^\infty dt C_T(q, t) \tag{2.7}$$

To see the consequences of this theory we take for the transverse current the hydrodynamic result $C_T(q, t) = Nmk_B T \exp[-(\eta/nm)q^2 t]$, and Eq. (6.7) becomes

$$D \approx (k_B T/4\pi\eta a) \equiv D_{\text{hyd}} \tag{6.8}$$

which is the Stokes-Einstein relation, with $a = [(4/3)\pi n]^{-1/3}$ playing the role of the particle radius, $R$. This is consistent with its earlier definition within the velocity field concept. Using experimental results for $\eta$, Eq. (6.8) is able to predict diffusion coefficients in fair agreement with measured values, especially at high densities. As one might expect, however, $R = a$ will tend to overestimate the effective particle radius and $D_{\text{hyd}}$ underestimate $D$.

If, instead of using the hydrodynamic form for $C_T(q, t)$, we apply the exact result given in Eq. (3.15), we obtain from (6.7)

$$D = (nk_B T/3\pi^2) \int_0^\infty dq \tilde{f}(q)/\eta(q) \tag{6.9}$$

In this expression, we have introduced a wavevector-dependent viscosity coefficient $\eta(q) \equiv \tilde{\eta}(q, z = 0)$. $D_{\text{hyd}}$ is obtained with $\eta(q) = \eta(0) \equiv \eta$, but in fact $\eta(q)$ is strongly dependent on $q$, and this must be taken into account when evaluating the integral in Eq. (6.9). A fully consistent theory of this $q$-dependence is still lacking, except at large wavevectors, where ideal gas theory gives

$$\eta(q \to \infty) = (2mn^2 k_B T/\pi)^{1/2} q^{-1} \tag{6.10}$$

To see the effect we can use the simple form $\eta(q) = \eta[1 + (Aq)^2]^{-1}$, with $A \approx 0.3\sigma$, which is a reasonable representation of rigid sphere computer data[113], except of course at large $q$. Substitution into Eq. (6.9) leads to $R = a/[1 + 2(A/a)^2]$, and

$$D = D_{\text{hyd}}[1 + 2(A/a)^2] \tag{6.11}$$

which corrects some of the deficiencies of the hydrodynamic treatment. The importance of the $q$-dependent visocity in this microscopic derivation of the Stokes-Einstein law indicates that the latter's apparent simplicity is somewhat deceptive. The concept of "particle radius" in the relationship between $D$ and $\eta$ contains a good deal of physical information. In this context, we point out that apart from the rigid sphere data of $\eta(q)$, there are computer simulation results for Ar[114] and Rb[115] models. In addition, data for the wavevector-dependent longitudinal viscosity has recently been deduced from the results of real experiments on Pb, Bi, and Rb[116]. There is some structure in the generalized viscosity, which is revealed by both computer and

**Table 6.1** Effective particle radius near the melting point.

| | $a$ (Å) | $\eta$ ($mP$) | $R = k_B T/4\pi\eta D$ (Å) | $a/R$ |
|---|---|---|---|---|
| Ar | 2.24 | 2.9 | 2.21 | 1.01 |
| $CH_4$ | 2.42 | 1.95 | 2.00 | 1.21 |
| Li | 1.75 | 6.0 | 1.21 | 1.45 |
| Na | 2.14 | 7.0 | 1.41 | 1.52 |
| K | 2.65 | 5.4 | 1.89 | 1.40 |
| Rb | 2.84 | 6.7 | 1.91 | 1.49 |
| Cs | 3.06 | 6.9 | 2.18 | 1.40 |
| Sn | 1.89 | 21.0 | 1.32 | 1.43 |

experiment, and for which there is no explanation at the present time. It has been demonstrated that it can have important consequences when $\eta(q)$ is used to calculate the self-diffusion coefficient[115].

In Table 6.1, values of the effective particle radius are compared with the atomic sphere radius for a number of simple liquids near the melting point. Experimental values of $D$ (Table 5.2) and $\eta$ are used.

The relatively small value of the ratio, $a/R$, for Ar is the result of choosing $D = 1.53 \times 10^{-5}$ cm$^2$ s$^{-1}$. This was obtained by means of a capillary method[39], but it should be pointed out that other workers have deduced a higher value for a state near the melting point. Corbett and Wang[40] obtain $D \approx 2.0 \times 10^{-5}$ cm$^2$ s$^{-1}$, which makes the ratio 1.32. Even so, the liquid metals are clearly distinguishable; note that for rigid spheres, near crystallization, $(a/R) \approx 1.27$, when $R = \sigma/2$.

## 7 CONCLUSIONS

Despite the long history of the subject, there is still a great deal to do in the area of atomic transport in liquids before we have a coherent picture of the way the transport mechanisms change with the thermodynamic parameters. We have, for example, pointed out the striking linear dependence of the fluidity of the liquid alkali metals on $\sqrt{T}$, along the saturated vapour pressure curve. The fluidity of liquid argon, on the other hand, does not have the same dependence on temperature. This may be due simply to the different way the volume changes with temperature in the two cases, but the reasons are not clear. On the positive side, the experimental evidence, generally, suggests that the concept of an activation energy is inappropriate and that a power law description of the data should be sought. (In this connection, we deplore the practice of reporting transport data by giving values for the parameters in an Arrhenius fit—tabulated results should always be given.) Because of experimental difficulties, self-diffusion data is rather sparse and there seems to be no consensus of the way $D$ varies with $T$. For argon, along the saturated vapour pressure curve the available evidence *suggests* a linear dependence on $T$. This can be said also of some liquid metal data. For metals particularly more extensive results are essential before any definite conclusions can be reached.

Since diffusion experiments are difficult molecular dynamics calculations of the self-diffusion coefficient in liquid metal-like systems are important, *provided that they are carried out in a systematic way.* More computer experiments along the saturated vapour pressure line, or alternatively along isochores and/or isotherms will be particularly valuable.

Although a theoretical framework is in place, and our knowledge of microdynamics in liquids has improved greatly over the last two decades, we still have to make further progress towards an understanding of the transport mechanisms and the way they depend on the interatomic forces. A convincing prediction of transport coefficients over wide ranges of temperature and density has still to be achieved. Mode-coupling theory offers hope of progress, although it has to be appreciated that the minimum requirement, as input data, is a knowledge of the structure of the liquid at each state point of interest. As an alternative to this difficult program, the rigid sphere fluid is exploited as a reference system (in much the same way as for the thermodynamics) from which to predict or correlate transport data in liquids. The problem here is to select an effective sphere diameter, and different ways of doing this have been discussed. The approach can be a useful way of correlating transport data when used in a systematic fashion[97].

A frequently used relationship in liquids (and supported by rigid sphere data) is the Stokes-Einstein equation connecting $D$ and $\eta$, although its original derivation gives no justification for its application in simple liquids. The introduction of a microscopic velocity field, to evaluate the velocity autocorrelation function, has thrown some light on the relationship. Not surprisingly within a microscopic framework a generalized transport coefficient, $\eta(q)$, appears in the theory, rather than a hydrodynamic coefficient. Nevertheless, the form of the equation remains intact, an effective particle radius being defined with in terms of $\eta(q)$.



*References*

1. J. P. Hansen and I. R. McDonald, *Theory of Simple Liquids*, 2nd. edn. (Academic Press, New York, 1986).
2. M. Ginoza and N. H. March, *Phys. Chem. Liq.*, **15**, 75 (1985).
3. J. Anderson and K. Saddington, *J. Chem. Soc.*, **152**, 381 (1949).
4. J. Crank, *The Mathematics of Diffusion*, 2nd. edn. (Clarendon Press, Oxford, 1975).
5. J. H. Wang, *J. Am. Chem. Soc.*, **73**, 510, 4181 (1952).
6. See for example, H. J. V. Tyrrell and K. R. Harris, *Diffusion in Liquids*, (Butterworth and Co. Ltd, 1984).
7. M. W. Ozelton and R. A. Swalin, *Phil. Mag.*, **18**, 441 (1968).
8. A. Lodding, S. Larsson, L. Broman and C. Roxbergh, *Z. Naturf. A* **25**, 1472 (1970).
9. D. A. Rigney, in "Liquid Metals, 1976", (R. Evans and D. A. Greenwood eds.) Institute of Physics (Bristol, 1977) p. 619.
10. T. Persson, P. E. Ericksson and L. Lindström, *J. Physique Suppl.*, **48**, C8 374 (1980).
11. J. S. Murday and R. M. Cotts, *J. Chem. Phys.*, **48**, 4938 (1968).
12. K. E. Larsson, *Phys. Chem. Liq.*, **12**, 273 (1982).
13. E. Donth and W. Ulrici, *Exptl. Tech. Physik*, **13**, 175 (1965).
14. L. Bewilogua and T. Yoshimura, *J. Low Temp. Phys.*, **8**, 255 (1972).
15. A. Uhlir, *J. Chem. Phys.*, **20**, 463 (1952).
16. L. D. Ikenberry and S. A. Rice, *J. Chem. Phys.*, **39**, 1561 (1963); B. J. Bailey and K. Kellner, *Physica*, **39**, 444 (1968); and references therein.
17. N. S. Rudenko and L. W. Schubnikov, *Physik. Z. Sowjetunion*, **6**, 470 (1934).
18. J. P. Boon, J. C. Legros and G. Thomaes, *Physica*, **32**, 1234 (1966).

19. J. Hellemans, H. Zink and O. Van Paemel, *Physica*, **46**, 395 (1970).
20. P. S. Van der Gulik and N. J. Trappeniers, *Physica*, **135A**, 1 (1986).
21. W. M. Haynes, *Physica*, **67**, 440 (1973); and references therein.
22. L. J. Wittenberg, D. Ofte and C. F. Curtiss, *J. Chem. Phys.*, **48**, 3253 (1968).
23. E. E. Shipil'rain, K. A. Yakimovich, V. A. Fomin, S. N. Skovorodjko and M. S. Mozgovoi, *Handbook of Thermodynamic and Transport Properties of Alkali Metals*, (R. W. Ohse ed.) (Blackwell Scientific Publications, Oxford, 1985) p. 753.
24. R. A. Fleury and J. P. Boon, *Phys. Rev.*, **186**, 244 (1969).
25. D. G. Naugle, J. H. Lunsford and J. R. Singer, *J. Chem. Phys.*, **45**, 4669 (1966).
26. S. V. Letcher and R. T. Beyer, *J. Acoust. Soc. Am.*, **35**, 1571 (1963), and references therein; K. G. Plass, *Acustica*, **13**, 240 (1963).
27. R. T. Beyer, *Handbook of Thermodynamic and Transport Properties of Alkali Metals*, (R. W. Ohse ed.) (Blackwell Scientific Publications, Oxford, 1985) p. 525.
28. K. C. Sharma, *Phys. Rev.*, **174**, 309 (1968).
29. E. N. da C. Andrade, *Phil. Mag.*, **17**, 698 (1934).
30. P. Taborek, R. N. Kleiman and D. J. Bishop, *Phys. Rev. B*, **34**, 1835 (1986).
31. A. J. Batschinski, *Z. Physik. Chem.*, **84**, 643 (1913).
32. J. H. Hildebrand, *Viscosity and Diffusivity*, (Wiley, New York, 1976).
33. J. J. Van Loef, *Physica*, **124B**, 305 (1984).
34. J. J. Van Loef, *Physica*, **75**, 115 (1974).
35. S. J. Larsson, C. Roxbergh and A. Lodding, *Phys. Chem. Liq.*, **3**, 137 (1972).
36. N. H. Nachtrieb, *Properties of Liquid Metals*, (P. A. Adams, H. A. Davies and S. G. Epstein eds.) (Taylor and Francis Ltd., London, 1967) p. 309.
37. R. E. Meyer and N. H. Nachtrieb, *J. Chem. Phys.*, **23**, 1851 (1955).
38. J. Naghizadeh and S. A. Rice, *J. Chem. Phys.*, **36**, 2710 (1962).
39. G. Cini-Castagnoli and F. P. Ricci, *Nuovo Cimento*, **15**, 795 (1960).
40. J. W. Corbett and J. H. Wang, *J. Chem. Phys.*, **25**, 422 (1956).
41. S. L. Ruby, J. C. Love, P. A. Flinn and B. J. Zabransky, *Appl. Phys. Lett.*, **27**, 320 (1975).
42. R. Zwanzig, in *Lectures in Theoretical Physics* vol. 111 (Wiley, New York, 1961) p. 135; H. Mori, *Prog. Theor. Phys.*, **33**, 423 (1965).
43. See. e.g. *Statistical Mechanics, Part B: Time-dependent Processes*, (B. J. Berne ed.) (Plenum, New York, 1977) p. 233.
44. M. S. Green, *J. Chem. Phys.*, **22**, 398 (1954) and *Phys. Rev.*, **119**, 829 (1960); R. Kubo, *J. Phys. Soc. Japan*, **12**, 570 (1957); E. Helfand, *Phys. Rev.*, **119**, 1 (1960).
45. R. Zwanzig, *Ann. Rev. Phys. Chem.*, **16**, p. 92 (1965).
46. A. Z. Akcasu and E. Daniels, *Phys. Rev. A*, **2**, 962 (1970).
47. P. Schofield in *The Physics of Simple Liquids*, (H. R. V. Temperley, J. S. Rowlinson and G. S. Rushbrooke, eds) (North-Holland, Amsterdam, 1968) chap. 13.
48. R. D. Mountain, *Adv. Mol. Relax. Processes*, **9**, 225 (1976).
49. D. J. Evans, *Phys. Rev. A*, **23**, 2622 (1981).
50. B. J. Alder, D. M. Gass and T. E. Wainwright, *J. Chem. Phys.* **53**, 3813 (1970).
51. B. J. Alder and T. E. Wainwright, *Phys. Rev. Letters*, **18**, 988 (1967).
52. J. J. Erpenbeck and W. W. Wood, *J. Stat. Phys.*, **24**, 455 (1981).
53. A. Rahman, *Phys. Rev.*, **136**, 405 (1964).
54. D. Levesque and L. Verlet, *Phys. Rev.* A, **2**, 2514 (1970).
55. M. Tanaka, *J. Phys. F*, **10**, 2581 (1980).
56. D. M. Heyes, *J. Chem. Soc. Faraday Trans.*, **79**, 1741 (1983).
57. D. Levesque, L. Verlet and J. Kurkijarvi, *Phys. Rev.*, A, 7 1690 (1973).
58. M. Schoen and C. Hoheisel, *Mol. Phys.*, **56**, 653 (1985).
59. D. Levesque and L. Verlet, *Mol. Phys.*, **61**, 143 (1987).
60. C. Hoheisel, R. Vogelsang and M. Schoen, *J. Chem. Phys.*, **87**, 7195 (1987).
61. R. Vogelsang, C. Hoheisel and G. Ciccotti, *J. Chem. Phys.*, **86**, 6371 (1987).
62. R. Vogelsang and C. Hoheisel, *Phys. Chem. Liq.*, **18**, 141 (1988).
63. L. M. Berezhkovsky, A. N. Drozdov, V. Yu. Zitserman, A. N. Lagar'kov and S. A. Tiger, *J. Phys. F*, **14**, 2315 (1984).
64. W. A. Harrison *Pseudopotentials in the Theory of Metals*, (Benjamin, New York, 1966).
65. R. Kumaravadivel, *J. Phys. F*, **13**, 1607 (1983).
66. N. W. Ashcroft, *Phys. Lett.*, **23**, 48 (1966).
67. U. Balucani, R. Vallauri and T. Gaskell, *Phys. Rev. A*, **37**, 3386 (1988); R. Vallauri (unpublished results).

68. Landolt-Börnstein, *Zahlenwerte und Funktionen*, 5 Teil (Springer, Berlin, 1969).
69. D. L. Price, K. S. Singwi and M. P. Tosi, *Phys. Rev. B*, **2**, 2983 (1970).
70. W. T. Ashurst and W. G. Hoover, *Phys. Rev.* A, **11**, 658 (1975).
71. G. Ciccotti and A. Tenenbaum, *J. Stat. Phys.*, **23**, 767 (1980); A. Tenenbaum, G. Ciccotti and R. Gallico, *Phys. Rev.* A, **25**, 2778 (1982); C. Trozzi and G. Ciccotti, *Phys. Rev.* A, **29**, 916 (1984).
72. M. Mareschal and E. Kestemont, *Phys. Rev.* A, **30**, 1158 (1984).
73. D. J. Evans, W. G. Hoover, B. H. Failor, B. Moran and A. J. C. Ladd, *Phys. Rev.*, A, **28**, 1016 (1983).
74. W. G. Hoover, D. J. Evans, R. B. Hickman, A. J. C. Ladd, W. T. Ashurst and B. Moran, *Phys. Rev.* A, **28**, 1016 (1983).
75. D. J. Evans and G. P. Morris, *Phys. Rev.* A, **30**, 1528 (1984).
76. A. W. Lees and S. F. Edwards, *J. Phys.* C, **5**, 1291 (1972).
77. D. J. Evans, *Phys. Lett.*, **A91**, 457 (1982); M. J. Gillan and M. Dixon, *J. Phys.* **C16**, 869 (1983).
78. D. J. Evans, in *Molecular Dynamics Simulation of Statistical Mechanical Systems*, (G. Cicotti and W. G. Hoover, eds) (North Holland, Amsterdam, 1986).
79. D. J. Evans, *Phys. Lett.* A, **74**, 229 (1979).
80. P. T. Cummings and C. P. Morriss, *J. Phys. F*, **17**, 593 (1987); ibidem, **18**, 1439 (1988).
81. G. Ciccotti, G. V. Paolini, J. P. Ryckaert and A. Bellemans, *Phys. Rev. Lett.*, **60**, 128 (1988).
82. C. Massobrio and G. Ciccotti, *Phys. Rev.* A, **30**, 3191 (1984); G. V. Paolini, G. Ciccotti and C. Massobrio, *Phys. Rev.* A, **34**, 1355, (1986).
83. D. M. Heyes, *Phys. Rev.* B, **37**, 5677 (1988).
84. N. W. Ashcroft and J. Leckner, *Phys. Rev.*, **145**, 83 (1966); J. A. Barker and D. Henderson, *J. Chem. Phys.*, **47**, 2856, 4714 (1967); L. Verlet, *Phys. Rev.*, **165**, 201 (1968).
85. A. A. Clifford and E. Dickinson, *Mol. Phys.*, **34**, 875 (1977).
86. J. P. Boon and S. Yip, *Molecular Hydrodynamics* (McGraw-Hill, 1980).
87. P. Schofield in *Molecular Motions in Liquids*, (J. Lascombe, ed) (D. Reidel, Dordrecht, 1974).
88. S. Chapman and T. G. Cowling, *The Mathematical Theory of Non-Uniform Gases* (Cambridge University Press, 1970); P. Resibois and De Leener, *Classical Kinetic Theory of Fluids* (John Wiley and Sons, New York, 1977).
89. P. Resibois, *J. Stat. Phys.*, **13**, 393 (1975).
90. R. J. Speedy, *Mol. Phys.*, **62**, 509 (1987).
91. E. Leutheusser, *J. Phys.* C, **15**, 2801 and 2827 (1982).
92. P. M. Furtado, G. F. Mazenko and S. Yip, *Phys. Rev.* A, **14**, 1653 (1976).
93. W. Sung and G. Stell, *J. Chem. Phys.*, **80**, 3350 and 3367 (1984).
94. J. H. Dymond, *J. Chem. Phys.*, **60**, 969 (1972) and *Physica*, **75**, 100 (1974).
95. A. F. Collings and E. McLaughlin, *Trans. Faraday Soc.*, **67**, 340 (1971).
96. M. A. McCool and L. A. Woolf, *J. Chem. Soc. Trans. Faraday* **1**, 340 (1971).
97. J. H. Dymond and T. A. Brawn, Proc. 7th Symp. Thermophys. Prop. Amer. Soc. Mech. Engnrs., (New York) 660 (1977).
98. P. Protopapas, H. C. Andersen and N. A. D. Parlee, *J. Chem. Phys.*, **59**, 15 (1973).
99. P. Protopapas, Master's Thesis in Metallurgy, Dept. Mineral Eng., Stanford University, 1972.
100. P. Ascarelli and A. Paskin, *Phys. Rev.*, **165**, 222 (1968).
101. T. Keyes, *Statistical Mechanics, Part B: Time-Dependent Processes*, (B. J. Berne, ed), (Plenum, New York, 1977) p. 259; G. F. Mazenko and S. Yip, ibidem, p. 181.
102. A. Sjölander, *Amorphous and Liquid Materials*, (E. Luscher, G. Fritsch and G. Jacucci, eds), (Martinus Nijhoff, 1987) p. 239.
103. T. Munakata and A. Igarashi, *Prog. Theor. Phys.*, **60**, 45 (1978).
104. D. Levesque and W. T. Ashurst, *Phys. Rev. Lett.*, **33**, 277 (1974).
105. Ch. Morkel, Ch. Gronemeyer and W. Gläser, *Liquid and Amorphous Metals*, (W. Gläser, F. Hensel and E. Lüscher, eds) (R. Oldenbourg Verlag, München, 1987) p. 357.
106. U. Balucani, R. Vallauri and T. Gaskell, *Phys. Rev. A*, **37**, 3386 (1988).
107. T. Geszti, *J. Phys. C*, **16**, 5805 (1983); U. Bengtzelius, W. Götze and A. Sjölander, *J. Phys. C*, **17**, 5915 (1984).
108. J. Bosse, W. Götze and M. Lücke, *Phys. Rev. A*, **17**, 434 and 447 (1978); ibidem, **18**, 1176 (1978); J. Bosse, W. Götze and A. Zippelius, ibidem, **18**, 1214 (1978).
109. L. Sjögren and A. Sjölander, *J. Phys. C*, **12**, 4369 (1979); L. Sjögren, *Phys. Rev. A*, **22**, 2866 and 2883 (1980).
110. T. Gaskell and S. Miller, *J. Phys. C*, **11**, 3749 (1978).
111. T. Gaskell and S. Miller, *J. Phys. C*, **11**, 4839 (1978); P. E. Mason and T. Gaskell, *Mol. Phys.*, **41**, 529 (1980); T. Gaskell, *J. Phys. C*, **16**, 381 (1986).
112. U. Balucani, R. Vallauri, T. Gaskell and M. Gori, *J. Phys. C*, **18**, 3133 (1985).

113. W. E. Alley and B. J. Alder, *Phys. Rev. A*, **27**, 3158 (1983).
114. T. Gaskell, U. Balucani, M. Gori and R. Vallauri, *Phys. Scripta*, **35**, 37 (1987).
115. U. Balucani, R. Vallauri and T. Gaskell, *Phys. Rev. A*, **35**, 4263 (1987).
116. K. E. Larsson and W. Gudowski, *Phys. Rev. A*, **33**, 1968 (1986).